

Quantum Energies of Strings in a 2+1 Dimensional Gauge Theory

N. Graham*

*Department of Physics, Middlebury College
Middlebury, VT 05753, USA*

M. Quandt†

*Institute for Theoretical Physics, Tübingen University
D-72076 Tübingen, Germany*

O. Schröder‡

*science+computing ag
Hagellocher Weg 73, 72070 Tübingen, FRG*

H. Weigel§

*Fachbereich Physik, Siegen University
D-57068 Siegen, Germany*

We study classically unstable string type configurations and compute the renormalized vacuum polarization energies that arise from fermion fluctuations in a 2+1 dimensional analog of the standard model. We then search for a minimum of the total energy (classical plus vacuum polarization energies) by varying the profile functions that characterize the string. We find that typical string configurations bind numerous fermions and that populating these levels is beneficial to further decrease the total energy. Ultimately our goal is to explore the stabilization of string type configurations in the standard model through quantum effects.

We compute the vacuum polarization energy within the phase shift formalism which identifies terms in the Born series for scattering data and Feynman diagrams. This approach allows us to implement standard renormalization conditions of perturbation theory and thus yields the unambiguous result for this non-perturbative contribution to the total energy.

PACS numbers: 03.65Sq, 03.70+k, 11.27+d

I. INTRODUCTION

In the past decades the perturbative treatment of the electroweak standard model has proven to be a very powerful tool to describe the properties and interactions of elementary particles within a wide energy regime. On the other hand the role and even the existence of non-perturbative solutions in this model is still quite uncertain. While the standard model does not contain topological solitons, one can construct nontopological string solutions to the classical equations of motion, called Z-strings or electroweak strings [1, 2, 3]. In the absence of topological arguments, however, one is not guaranteed that these classical solutions actually correspond to true local minima of the full effective energy, or even the classical energy. Indeed, Naculich [4] has shown that in the limit of weak coupling, fermion fluctuations destabilize the string solution. This analysis leaves open the possibility, however, that deformed string solutions could exist, which would be local minima of the full effective energy. Since fermions are tightly bound in the string background, one potential mechanism for restoring stability is for fermions to bind to the string, yielding a lower total energy than a corresponding density of free fermions. When including this effect, however, one must also take into

*Electronic address: ngraham@middlebury.edu

†Electronic address: quandt@tphys.physik.uni-tuebingen.de

‡Electronic address: oliver.schroeder@science-computing.de

§Electronic address: weigel@physik.uni-siegen.de

account the shifts in the zero-point energies of all the unoccupied modes as well, computed consistently in a standard renormalization scheme.

If stabilized by the fermion binding mechanism, electroweak strings could have significant cosmological consequences [5, 6]. A network of strings could contribute to the dark energy that is required to explain the recently observed cosmic acceleration [7, 8]. However, a complete dynamical description of that scenario is still missing [9, 10, 11]. Also, as pointed out by Nambu [3], Z -strings are expected to terminate in monopole–antimonopole pairs, which could give rise to a primordial magnetic field. Furthermore, a network of stable strings at the electroweak phase transition would provide a scenario for electroweak baryogenesis without requiring a first-order phase transition [12]. The strings provide out-of-equilibrium regions, and the core of the string has copious baryon number violation due to the suppressed Higgs condensate. They thus provide an alternative to the usual idea of bubble–nucleation baryogenesis, which requires a first order phase transition to go out of thermal equilibrium.

From a theoretical point of view, the quantum properties of Z -strings have been connected to non-perturbative anomalies [13]. Decoupling arguments [14, 15] suggest that when a fermion’s mass is made very large by increasing its Yukawa coupling, soliton configurations should appear in the low-energy spectrum to maintain cancellation of such anomalies. In these calculations, the analysis of the fermion determinant – whose logarithm is the sum over zero-point energies – is essential.

A first attempt at a full calculation of the quantum corrections to the Z -string energy was carried out in [16]. Those authors were only able to compare the energies of two string configurations, rather than comparing a single string configuration to the vacuum. Furthermore, they used a proper time prescription, in which it was not possible to explicitly split off the divergent parts from the fermion determinant. Thus the final answer was expressed at large but finite cut-off in terms of two large terms that could only be computed numerically, representing the fermion determinant and the counterterms. In this formulation, no numerically stable results could be extracted for the limit “cut-off to infinity.” In the present work, we will employ phase shift techniques [17], which allow us to make this separation cleanly and unambiguously.

In this paper we restrict ourselves to the case of $2 + 1$ dimensions. We make this restriction to simplify the renormalization procedure. However, from the experience gathered in the case of QED magnetic flux tubes [18], it is reasonable to expect that the qualitative behavior might be very similar to the actual $3+1$ dimensional theory. The techniques of [19] allow for a straightforward generalization of the calculational procedure used here to that case as well. We also consider only the weak interactions, neglecting electromagnetism. Although introducing electromagnetism into our calculation is not entirely straightforward because of the effects of Aharonov-Bohm phases discussed in ref. [18], we expect the approach of that paper to provide a natural generalization to the full electroweak interactions. In particular, the symmetry operator we rely on for the partial wave decomposition of our phase shifts continues to hold in the full theory.

The paper is organized as follows. In Section II we will consider the Higgs–gauge sector model, consisting of a doublet Higgs coupled to an $SU(2)$ gauge field, and discuss various aspects of classical string configurations. In Section III we discuss the coupling of the fermions to string configurations and compute the energy that arises from summing the fermion zero modes. We will present our numerical results for the corrected string energy in Section IV. Some preliminary results of the current investigation were reported in conference proceedings [20].

II. THE HIGGS–GAUGE–SECTOR

Our principal aim is to study string-like configurations within the standard electroweak $SU(2) \times U(1)$ model. In the present paper, we will consider a simplified version of this theory, in which

1. the spacetime dimension is reduced to $D = 2 + 1$ or, equivalently, bosonic configurations are translationally invariant in the third space direction,
2. the Weinberg angle, θ_W is set to zero, *i.e.* the $U(1)$ factor in the gauge group decouples (and will be discarded in the following). The classical energy actually decreases when θ_W is turned on in the full theory. Hence a configuration that is stable at $\theta_W = 0$ most likely is also stable otherwise. And
3. quantum corrections to the bosonic string configurations are taken from the fermion sector only; this approximation may be justified in situations where the degeneracy of the fermion modes (e.g. the number of colors N_C) is large.

The action of the simplified model consists of two parts, $S = S_H + S_F$, where the bosonic (Higgs-gauge) sector S_H is treated *classically* and the fermion part gives rise to quantum fluctuations around bosonic field configurations. In the present section, we discuss properties of classical string-like configurations in the bosonic sector while the quantum treatment of the fermions is deferred to section III.

The Higgs-gauge sector S_H in our model reads

$$S_H[\phi, W] = \int d^3x \left[-\frac{1}{2} \text{tr} (G^{\mu\nu} G_{\mu\nu}) + (D^\mu \phi)^\dagger D_\mu \phi - \lambda (\phi^\dagger \phi - v^2)^2 \right]. \quad (2.1)$$

We work in $D = 2 + 1$ spacetime with Minkowski signature and include the gauge coupling strength, g , explicitly in all vertices. Thus, the field strength tensor is given by

$$G_{\mu\nu} = \partial_\mu W_\nu - \partial_\nu W_\mu - ig [W_\mu, W_\nu], \quad (2.2)$$

where the three $SU(2)$ vector bosons, W_μ^a , are components of a Lie-algebra valued matrix connection,

$$W_\mu = W_\mu^a \frac{\tau^a}{2} \equiv W_\mu^a T^a. \quad (2.3)$$

As indicated, we use hermitian generators $T^a = \tau^a/2$ (where τ^a are the Pauli matrices) with the commutation relation $[T^a, T^b] = i\epsilon^{abc} T^c$. The complex scalar Higgs field is in the fundamental representation of $SU(2)$,

$$\phi = \begin{pmatrix} \phi_+ \\ \phi_0 \end{pmatrix} \quad (2.4)$$

while the covariant derivative contains the Higgs-gauge coupling constant g explicitly,

$$D_\mu \phi = (\partial_\mu - ig W_\mu) \phi. \quad (2.5)$$

By construction, the action eq. (2.1) is invariant under $SU(2)$ gauge rotations $V = \exp(i\theta^a(x)T^a)$,

$$\phi \rightarrow V\phi \quad \text{and} \quad ig W_\mu \rightarrow V (-\partial_\mu + ig W_\mu) V^\dagger. \quad (2.6)$$

For positive values of the self-coupling $\lambda > 0$, the Higgs doublet acquires a vacuum expectation value (VEV) conventionally chosen as¹

$$\langle \phi_0 \rangle = v, \quad \langle \phi_+ \rangle = 0.$$

As a consequence, the system undergoes complete spontaneous symmetry breaking $SU(2) \rightarrow \{1\}$, i.e. there is no group generator that leaves the vacuum invariant. As a consequence, there are three would-be Goldstone modes from ϕ fluctuations, which become longitudinal modes of the gauge field as it acquires a mass $M_W = gv/\sqrt{2}$ (at tree level). The remaining Higgs excitations are also massive with a (tree-level) mass of $M_H = 2v\sqrt{\lambda}$.

In the course of this paper it will occasionally be convenient to re-write the covariant derivative, eq. (2.5) as

$$D_\mu \phi = [\partial_\mu - ig Q_Z Z_\mu - ig (W_\mu^+ T^- + W_\mu^- T^+)] \phi, \quad (2.7)$$

where the charge operators and fields are

$$\begin{aligned} Q_Z &= \frac{1}{2} \tau^3 & T^\pm &= \frac{1}{\sqrt{2}} (\tau^1/2 \pm i\tau^2/2) \\ Z_\mu &= W_\mu^3 & W_\mu^\pm &= \frac{1}{\sqrt{2}} (W_\mu^1 \pm iW_\mu^2). \end{aligned} \quad (2.8)$$

We will use the notation W_μ^3 and Z_μ interchangeably.

¹ In the full $SU(2) \times U(1)$ model, this choice ensures that the unbroken $U(1)$ group is generated by the electric charge $Q = I_w^3 + Y_W/2$, where I_w and Y_W are weak isospin and hypercharge, respectively.

A. The Classical String Solutions

Our main interest is in string-like configurations of the bosonic sector. We analyze the energy of (classical) localized configurations in two space dimensions. A subsequent extension of this analysis would be to consider configurations in three dimensions that are translationally invariant in the z direction, with a finite energy per unit length in a localized region of the $x - y$ plane. The region in which the energy density is concentrated would thus take the form of a tube extending along the z -axis. Such field configurations are commonly called *cosmic strings* to distinguish them from the fundamental objects in string theory. In the present paper, we will refer to these objects simply as *strings* or *vortices*.

Finite energy requires the configuration to be pure gauge at spatial infinity. Let (ρ, φ) denote the radial and angular coordinates in the plane. At $\rho \rightarrow \infty$, the most general vacuum configuration is

$$\phi^{(\infty)} = V \begin{pmatrix} 0 \\ v \end{pmatrix} \quad \text{and} \quad gW_\mu^{(\infty)} = iV\partial_\mu V^\dagger, \quad (2.9)$$

where the $SU(2)$ rotation $V(\varphi)$ maps the circle S_1 at infinity onto the gauge group G . For the electromagnetic case $G = U(1)$, such maps would be characterized by an integral winding number $\Pi_1(U(1)) = \mathbb{Z}$ and we would obtain topologically stable Nielsen–Olesen vortices [21]. However, the weak isospin group in our model is $G = SU(2)$. We can still embed Nielsen–Olesen type solutions in this larger gauge group by considering maps from the spatial boundary S_1 to various $U(1)$ subgroups of $G = SU(2)$. There is, of course, considerable arbitrariness in this procedure, since no $U(1)$ subgroup survives the electroweak symmetry breaking, so there is no ‘natural’ candidate for the target $U(1)$. Moreover, from $\Pi_1(SU(2)) = 0$, no such embedded string configuration is *topologically stable* against deformations in the full $SU(2)$ group; this will be discussed in more detail in section II B.

First we consider the $U(1)$ subgroup generated by the charge Q_Z associated with the neutral W_μ^3 (or Z_μ) gauge fields, as defined in eq. (2.8). In the full $SU(2) \times U(1)$ electroweak theory, Q_Z becomes the charge of Z_μ , the gauge field that couples to the weak neutral current, and the vortex associated with Q_Z becomes the *Z-string*. The maps that specify the asymptotic pure-gauge configurations are

$$V(\varphi) = e^{-2in\varphi Q_Z}, \quad (2.10)$$

where n must be integral to obtain single-valued Higgs fields. To construct the corresponding vortex configuration, we first adopt the Weyl gauge

$$W_0^a = 0.$$

In non-Abelian gauge theories, there might be topological obstructions to implementing this gauge [22, 23]; such defects are, however, associated with non-trivial (periodic) boundary conditions in the *time* direction. For static configurations, no such obstructions exists and the Weyl gauge may always be attained; the residual gauge freedom consists of all time-independent gauge rotations. We shall adopt this gauge throughout the rest of the paper.

The explicit form of the W^3/Z -string now dwells in the neutral component of the gauge field ($\hat{\varphi}$ is the unit vector in azimuthal direction)

$$\phi_0 = v f_H(\rho) e^{in\varphi} \quad \text{and} \quad \vec{W}^3 = \frac{2n}{g\rho} f_G(\rho) \hat{\varphi}, \quad (2.11)$$

with all other fields vanishing. The radial functions f_H and f_G must vanish at the origin to avoid singularities, and approach unity at infinity to have finite energy. Substituting this *ansatz* into the action, eq. (2.1), yields the classical energy

$$E_{\text{cl}} = 2\pi \int_0^\infty d\rho \rho \left[\frac{2}{g^2} \left(\frac{f'_G}{\rho} \right)^2 + v^2 (f'_H)^2 + \frac{v^2}{\rho^2} f_H^2 (1 - f_G)^2 + \lambda v^4 (1 - f_H^2)^2 \right]. \quad (2.12)$$

Minimizing this energy functional leads to the Nielsen–Olesen differential equations

$$\begin{aligned} 0 &= f_H'' + \frac{1}{\rho} f_H' - \frac{n^2}{\rho^2} f_H (1 - f_G)^2 + 2\lambda v^2 f_H (1 - f_H^2), \\ 0 &= f_G'' - \frac{1}{\rho} f_G' + \frac{1}{2} (g^2 + g'^2) v^2 f_H^2 (1 - f_G), \end{aligned} \quad (2.13)$$

which can be integrated numerically. Near the origin $\rho \rightarrow 0$, the radial functions behave as

$$f_H(\rho) \propto \rho \quad \text{and} \quad f_G(\rho) \propto \rho^2. \quad (2.14)$$

Notice finally that our W^3/Z -vortex carries quantized magnetic flux associated with the Abelian charge Q_Z . Defining the pseudoscalar magnetic field $B = \partial_x W_y^3 - \partial_y W_x^3$, we have

$$F = \int d^2x B = \frac{4\pi n}{g}. \quad (2.15)$$

This flux would flow along the vortex tube in $D = 3 + 1$ dimensions. The classical energy density creates a pressure that tends to spread out the flux, while the Higgs condensate is suppressed in the region of non-vanishing B , which tends to compress the flux. As a result of these two competing effects, the W^3/Z -string is stabilized at an equilibrium thickness.

In the above exploration we have chosen to embed the string in the $W^3/Z-U(1)$ submanifold. This choice, however, is arbitrary. For example, we could equally well chose a family of $U(1)$ submanifolds that is defined by the generator $\hat{n} \cdot \vec{T}$ where \hat{n} is a unit vector.

In addition to strings carried by the neutral gauge field, there are also string-like configurations that live entirely in the *charged* sector with $Z_\mu \equiv 0$.

B. Connecting Strings to Vacua: The Sphaleron Square

String solutions are characterized by the homotopy group $\Pi_1(G)$ of their boundary condition (2.9) at spatial infinity. Since $\Pi_1(SU(2)) = 0$, no topologically stable string solutions exists in our model (nor in the full electroweak theory). In other words, the string solution can be continuously deformed into the vacuum with finite energies along the entire path of deformation. In the following we will consider such deformation paths, because they represent the starting point for a variational approach to minimize the string energy when the vacuum polarization from the fermion sector is included.

1. String deformations

We construct non-contractible two-parameter loops of configurations with W-strings as the top of the tightest loop [24, 25]: Let β_1, β_2, α denote angular coordinates which describe a three-dimensional sphere, S_3 , with $0 \leq \beta_i \leq \pi$ and $0 \leq \alpha < 2\pi$. The sphere S_3 can be embedded as a unit sphere in a four-dimensional Euclidean space and is described by unit vectors

$$\hat{n}(\beta_1, \beta_2, \alpha) = \begin{pmatrix} \sin \beta_1 \sin \beta_2 \cos \alpha \\ \cos \beta_1 \\ \sin \beta_1 \cos \beta_2 \\ \sin \beta_1 \sin \beta_2 \sin \alpha \end{pmatrix}. \quad (2.16)$$

First, a map with unit winding number from S_3 to $SU(2)$ is given by

$$U^{(1)}(\beta_1, \beta_2, \alpha) = \hat{n}_0 \mathbb{1} - i \hat{n} \cdot \vec{\tau}. \quad (2.17)$$

To construct a map with winding number n , we may either raise the above $U^{(1)}$ to the power of n or, even simpler, scale the azimuthal angle α of $U^{(1)}$ [26],

$$U^{(n)}(\beta_1, \beta_2, \alpha) = U^{(1)}(\beta_1, \beta_2, n\alpha). \quad (2.18)$$

If we now identify the S_1 subspace spanned by α with the circle at infinity in the spatial $x - y$ plane (*i.e.* we set $\varphi = \alpha$), we obtain a two-parameter family of maps characterizing possible string boundary conditions (2.9):

$$U_{\xi_1, \xi_2}(\varphi) = U^{(n)}(\xi_1, \xi_2, \varphi). \quad (2.19)$$

As before, we construct string configurations with these boundary conditions by dressing the asymptotic form, eq. (2.9), with appropriate radial functions,

$$\phi = f_H(\rho) U_{\xi_1, \xi_2}(\varphi) \begin{pmatrix} 0 \\ v \end{pmatrix} \quad \text{and} \quad \vec{W} = \frac{1}{g} \frac{\hat{\varphi}}{\rho} f_G(\rho) U_{\xi_1, \xi_2}(\varphi) \partial_\varphi U_{\xi_1, \xi_2}^\dagger(\varphi), \quad (2.20)$$

The radial functions go from zero at the origin (to ensure smoothness) and to unity at infinity (to ensure finite energy). Substituting the explicit expression for U_{ξ_1, ξ_2} , we get

$$\begin{aligned}\phi &= v f_H(\rho) \begin{pmatrix} -i \cos \xi_1 - \sin \xi_1 \cos \xi_2 \\ \sin \xi_1 \sin \xi_2 e^{in\varphi} \end{pmatrix} \\ \vec{W}^3 &= \frac{2n}{g\rho} \hat{\varphi} f_G(\rho) \sin^2 \xi_1 \sin^2 \xi_2, \\ \vec{W}^+ &= \frac{\sqrt{2}n}{g\rho} \hat{\varphi} e^{-in\varphi} f_G(\rho) \sin \xi_1 \sin \xi_2 (i \cos \xi_1 + \sin \xi_1 \cos \xi_2). \end{aligned} \quad (2.21)$$

For $\xi_1 = \xi_2 = \pi/2$, we have the W^3/Z -string configuration with the radial functions satisfying the Nielsen-Olesen differential equations. On the boundary of the square spanned by ξ_1 and ξ_2 , all fields are zero except for the charged scalar ϕ_+ , which takes the form:

$$\begin{aligned}\xi_1 = 0: \quad \phi_+ &= iv f_H(\rho), & \xi_1 = \pi: \quad \phi_+ &= -iv f_H(\rho), \\ \xi_2 = 0: \quad \phi_+ &= iv e^{-i\xi_1} f_H(\rho), & \xi_2 = \pi: \quad \phi_+ &= iv e^{i\xi_1} f_H(\rho). \end{aligned} \quad (2.22)$$

To summarize, we have a two-parameter family of finite-energy string configurations that we will refer to as the *sphaleron square*. The center of the square at $(\xi_1 = \xi_2 = \pi/2)$ corresponds to the W^3/Z -string discussed earlier. From the W^3/Z -string we may go to any point on the boundary of the square (say $\xi_1 = 0$) and then deform $f_H(\rho)$ smoothly to unity everywhere so as to finally reach a vacuum configuration. The energy remains finite during the entire deformation. In fact, the energy density on the sphaleron square is

$$\mathcal{E}_{\text{cl}} = \left[\frac{2}{g^2} \left(\frac{f'_G}{\rho} \right)^2 + \frac{v^2}{\rho^2} f_H^2 (1 - f_G)^2 \right] n^2 \sin^2 \xi_1 \sin^2 \xi_2 + v^2 (f'_H)^2 + \lambda v^4 (1 - f_H^2)^2, \quad (2.23)$$

which is maximal at the W^3/Z -string, thereby justifying the “sphaleron” designation. Note that it is possible to extend this construction to the full electroweak theory; this approach will be used in a forthcoming study on the Z -string in 3+1 dimensions.

2. Charged scalar condensate

We make one simple expansion of the sphaleron square ansatz by introducing an additional radial function for the upper component of the scalar field. We will observe below that such an extension is necessary to avoid technical problems when integrating the second order Dirac equation for fermions in the string background, cf. sec. III F. In addition, this modification allows us to probe the stability with respect to variations in the upper Higgs component. So our full *ansatz* for the string background in the bosonic sector reads:

$$\begin{aligned}\phi &= v \begin{pmatrix} f_H(\rho)(-i \cos \xi_1 - \sin \xi_1 \cos \xi_2) + f_P(\rho) \\ f_H(\rho) \sin \xi_1 \sin \xi_2 e^{in\varphi} \end{pmatrix}, \\ \vec{W}^3 &= \frac{2n}{g\rho} \hat{\varphi} f_G(\rho) \sin^2 \xi_1 \sin^2 \xi_2, \\ \vec{W}^+ &= \frac{\sqrt{2}n}{g\rho} \hat{\varphi} e^{-in\varphi} f_G(\rho) \sin \xi_1 \sin \xi_2 (i \cos \xi_1 + \sin \xi_1 \cos \xi_2), \end{aligned} \quad (2.24)$$

where $f_P(\rho)$ is non-zero at the origin and goes to zero as $\rho \rightarrow \infty$. The magnitude of the Higgs field takes a simple form along the line $\xi_2 = \pi/2$,

$$|\phi|^2 = f_H^2 + f_P^2. \quad (2.25)$$

In the following, we shall restrict our variational search to $\xi_2 = \pi/2$. The additional Higgs component then contributes

$$\Delta \mathcal{E}_{\text{cl}} = v^2 \left[f_P'^2 + \frac{n^2}{\rho^2} f_P^2 f_G^2 \sin^2 \xi_1 \right] + v^4 f_P^2 [f_P^2 + 2f_H^2 - 2] \quad (2.26)$$

to the energy density, eq. (2.23).

III. FERMIONS ON STRINGS

As we have seen in the last section, electroweak strings are classically unstable. It is conceivable, however, that their quantum interactions with leptons and quarks might lead to stabilization: Since the Higgs condensate is suppressed in the vortex core, the fermions become effectively massless on the string, so energy can be gained by populating these states. If the energy gain is large enough, the string ceases to decay and it becomes a stable multi-quark object with a potentially rich phenomenology [5, 6].

To treat the fermions consistently, we not only have to consider the bound states but also the full Dirac sea, *i.e.* the fermion vacuum polarization, E_{vac} . This quantity is the most cumbersome part of the computation and to our knowledge, it has not been calculated properly before. The main difficulty arises because the (string) background is of non-perturbative nature while the renormalization conditions are formulated within perturbation theory. In this chapter we will discuss our approach to this issue in greater detail.

Let us assume that N_f fermions (with perturbative mass m_f) are trapped along the string by occupying N_f of the bound states that are induced by the string background. These bound states are characterized by energy eigenvalues² $0 \leq \epsilon_i < m_f$. The explicit occupation of N_f bound states then contributes

$$E_{\text{occ}}^{(N_f)} = \sum_{i=1}^{N_f} \epsilon_i \quad (3.1)$$

to the total energy. It is, of course, clear that the minimal total energy is found if we occupy the N_f *lowest* bound states in eq. (3.1). The total energy associated with fermion number N_f is then

$$E_{\text{eff}}^{(N_f)} = E_{\text{cl}} + E_{\text{occ}}^{(N_f)} + E_{\text{vac}}. \quad (3.2)$$

We emphasize that $E_{\text{occ}}^{(N_f)}$ and E_{vac} are formally of the same order in \hbar , and the inclusion of either thus requires the other. The effective energy $E_{\text{eff}}^{(N_f)}$ must be compared with the mass of N_f elementary (perturbative) fermions, *i.e.* stabilization occurs if

$$E_{\text{eff}}^{(N_f)} < m_f N_f. \quad (3.3)$$

Our main goal is to perform a variational search in our string *ansatz* space, so as to minimize $E_{\text{eff}}^{(N_f)}$ until eq. (3.3) holds. It is immediately evident that certain situations will be favorable *a priori*:

1. The perturbative fermion should be as heavy as possible; we will therefore concentrate on the top quark contribution to $E_{\text{eff}}^{(N_f)}$.
2. If fermions carry an internal degree of freedom (*e.g. color*) and N_C is the corresponding degeneracy, then both $E_{\text{occ}}^{(N_f)}$ and E_{vac} acquire a factor N_C , whereas E_{cl} does not. Thus a large color degeneracy enhances the quantum piece of the total energy. The fermion number with internal degeneracy is then $(N_f N_C)$, and the stability criterion eq. (3.3) becomes $E_{\text{eff}}^{(N_f)} < m_f (N_f N_C)$.

A. The Theory

We ignore inter-generation mixing and set the CKM matrix to unity. For simplicity, we shall also assume that fermions within an isospin doublet are degenerate. This simplifying assumption is violated in reality (in particular for the heavy quarks), but it gives us an additional symmetry which we need to make the calculation of E_{vac} manageable. Let us therefore consider one degenerate isospin doublet Ψ of heavy fermions (*e.g.* the top-bottom pair). In $D = 2 + 1$ the action for the doublet is

$$S_F[\Psi, \Phi, W_\mu] = \int d^3x \left[\bar{\Psi} i \gamma^\mu D_\mu P_L \Psi + \bar{\Psi} i \gamma^\mu \partial_\mu P_R \Psi - f \bar{\Psi} (\Phi P_R + \Phi^\dagger P_L) \Psi \right], \quad (3.4)$$

² Our background profiles lead to CP invariant interactions for the fermions, cf. sec. III F. It is therefore sufficient to consider non-negative energy eigenvalues and positive fermion numbers N_f .

where

$$P_{L,R} = \frac{1 \mp \gamma^5}{2} \quad \text{and} \quad \Phi = \begin{pmatrix} \phi_0^* & \phi_+ \\ -\phi_+^* & \phi_0 \end{pmatrix}. \quad (3.5)$$

The degeneracy of the isospin doublet is reflected by the appearance of a single Yukawa coupling constant, f . The corresponding fermion mass,

$$m_f = fv \quad (3.6)$$

is generated as usual from spontaneous symmetry breaking via the Higgs VEV. The coupling to the gauge fields appears through the covariant derivative, which takes the same form as eq. (2.5), except that the gauge fields W_μ only couple to the left-handed fermions $P_L \Psi$ (as in the full electroweak theory). Finally, we employ 4-component Dirac spinors even in $D = 2 + 1$ to mimic the full $D = 3 + 1$ calculation as closely as possible. Including the two isospin degrees of freedom, our fermion spinors Ψ thus have 8 complex components.

B. The Effective Energy

In path integral language, the vacuum polarization energy is obtained by integrating out the heavy fermion doublet. For this purpose, we decompose the fermion action (3.4) into the free part and the interaction with the bosonic background fields. The latter enters in the form of a background potential, $U = U(W, \Phi)$,

$$S_F[\Psi, W_\mu, \Phi] = \int d^3x [\bar{\Psi}(i\gamma^\mu \partial_\mu - m_f \mathbb{1})\Psi - \bar{\Psi} U(W, \Phi) \Psi], \quad (3.7)$$

which may easily be extracted from eqs. (3.4) and (3.5). If we normalize the fermion loop contribution to the boson action by subtracting off the result in the free non-interacting case, a formal path integral expression would be

$$S_q[W, \Phi] \equiv S_q[U] = (-i) \log \frac{\int d[\Psi, \bar{\Psi}] \exp(iS_F[\Psi, U])}{\int d[\Psi, \bar{\Psi}] \exp(iS_F[\Psi, U=0])}. \quad (3.8)$$

In the language of Feynman diagrams, eq. (3.8) equals the sum of all graphs with one fermion loop and an arbitrary number of $(-iU)$ insertions, *i.e.*

$$S_q[U] = \sum_{n=1}^{\infty} S_{\text{FD}}^{(n)}[U]. \quad (3.9)$$

Notice that the $n = 0$ term (corresponding to a cosmological constant) is not included due to our normalization eq. (3.8). As it stands, eq. (3.9) is, of course, ill-defined due to severe UV divergences in the low-order Feynman diagrams. We can identify these divergent graphs by power counting and assign a definite value to them using a specific regularization method that introduces a regulator (for instance a momentum cut-off, Λ , or the deviation, ϵ , from the physical dimension). Next, we cancel the divergences by adding counterterms to the initial (tree-level) boson Lagrangian. If the regularization method respects the *gauge invariance* of the fermion loop, the counterterms will be gauge invariant, too.³ Moreover, since our model is renormalizable, the counterterms are local monomials in the boson fields of mass dimension four or less. With these constraints, the most general counterterm Lagrangian in the Higgs-gauge sector reads

$$\mathcal{L}_H^{(\text{ct})} = c_1 \text{tr}(G^{\mu\nu} G_{\mu\nu}) + c_2 [D^\mu \phi]^\dagger D_\mu \phi + c_3 [(\phi^\dagger \phi) - v^2] + c_4 [(\phi^\dagger \phi) - v^2]^2. \quad (3.10)$$

After adding this term to the initial Lagrangian eq. (2.1) and replacing all fields and couplings by the renormalized ones,⁴ the fermion loop calculation is now based on the starting bosonic Lagrangian $\mathcal{L}_H^{(\text{ren})} + \mathcal{L}_H^{(\text{ct})}$. The counterterm coefficients c_i are of order $\mathcal{O}(\hbar)$ and enter the one-loop effective action directly,

$$S_{\text{eff}}^{(\text{ren})}[W, \Phi] = S_H[W, \Phi] + \left(S_H^{(\text{ct})}[W, \Phi] + \sum_{n=1}^{\infty} S_{\text{FD}}^{(n)}[U] \right) \equiv S_H[W, \Phi] + S_{\text{vac}}[W, \Phi]. \quad (3.11)$$

³ This statement is more subtle when boson loops are included. In this case, the gauge fixing requirement only leaves a global BRS invariance of the bare action, which does *not* translate directly into BRS invariant counterterms.

⁴ If the context does not lead to confusion, we will use the same notation for renormalized and bare fields/parameters.

We can adjust the coefficients c_i such that they cancel the divergences in the low order Feynman diagrams. The remaining (finite) arbitrariness is fixed by imposing specific renormalization conditions on Green's functions at prescribed external momenta (discussed in more detail in section III D). Although there is no unique specification of the theory by renormalized parameters, we prefer to choose a scheme where these quantities take *empirical* values that may, in principle, be determined from experiment; a complete list is given in the next subsection.

The discussion above concentrated on the effective action. For static boson fields, all these statements translate rather trivially into expressions for the energy: We simply have to replace $S \rightarrow E \equiv -\lim_{T \rightarrow \infty} S/T$, where T is the time extension of our fields. For instance, the one-loop effective action gives rise to a one-loop quantum energy

$$E_{\text{eff}}[W, \Phi] \equiv E_{\text{cl}}[W, \Phi] + E_{\text{vac}}[W, \Phi] = -\lim_{T \rightarrow \infty} T^{-1} S_{\text{eff}}^{(\text{ren})}[W, \Phi] \quad (3.12)$$

where E_{cl} refers to the classical energy of the Higgs–gauge sector, *cf.* eq. (2.23). The vacuum polarization piece in eq. (3.12) has two parts, the total fermion loop correction (3.9) (with the replacement $S \rightarrow E = -S/T$) and the counterterm contribution

$$E_{\text{ct}}[W, \Phi] = \int d^2x \left\{ -c_1 \text{tr}(W_{ij}W_{ij}) + c_2 [D_i \phi]^\dagger D_i \phi - c_3 [(\phi^\dagger \phi) - v^2] - c_4 [(\phi^\dagger \phi) - v^2]^2 \right\}. \quad (3.13)$$

It should be emphasized again that only the *sum* of these two parts is finite as the regulator is removed, *e.g.* $\Lambda \rightarrow \infty$ or $\epsilon \rightarrow 0$. One of the main advantages of our method is that the two contributions to E_{vac} are manifestly combined such that no explicit cutoff is required even at intermediate stages of the calculation.

Besides the classical, vacuum polarization and counterterm piece, a given configuration with fermion number N_f will also have to include a contribution from explicitly occupied bound states,

$$E_{\text{eff}}^{(N_f)}[W, \Phi] = E_{\text{cl}}[W, \Phi] + E_{\text{occ}}^{(N_f)}[W, \Phi] + E_{\text{vac}}[W, \Phi]. \quad (3.14)$$

This is the quantity to be used for the main stability criterion eq. (3.3). In the following subsections, we will discuss the individual ingredients into our main formula (3.14) in more detail.

To close this section, a brief comment is in order: We are well aware that a consistent one-loop calculation must include gauge and Higgs field loops, too. However, we choose to ignore these contributions in the present calculation, since our main motivation is slightly different: We are mainly concerned with the study of fermion effects on bosonic backgrounds. A consistent treatment of the fermion sector requires the inclusion of both bound state and sea quark contributions. Although bosonic loops also appear at the same order in \hbar , they are suppressed compared to the fermionic fluctuations by a factor of the number N_C of internal fermion degrees of freedom (*e.g.* color). Our approximation is relevant when N_C can be assumed to be large, becoming exact in the limit $N_C \rightarrow \infty$, since all boson lines in Feynman diagrams are suppressed in this case.

C. Theory Parameters

As mentioned earlier, we choose to define our model by renormalized parameters that have, in principle, a direct relation to electroweak phenomenology. However, our model is defined in two space dimensions so that the (dimensionful) gauge coupling constant g can no longer be expressed in terms of the Fermi constant $G_F \approx 10^{-5} m_{\text{proton}}^{-2}$ via the standard relation $G_F/\sqrt{2} = g^2/M_W^2 = 2/v^2$. To see which value of v should be chosen in $D = 2 + 1$, consider the classical energy (or energy per unit length) in eq. (2.23). In any number of dimension this quantity takes the form v^2 times a dimensionless function involving only ratios of masses. Thus the mass dimension comes from the prefactor v^2 only, which must therefore be adjusted such that the known $D = 3 + 1$ value of v^2 is multiplied by an appropriate length scale. Since we relate all dimensionful quantities to the mass m_f of the heavy fermion, one might expect that the appropriate length scale is the Compton wave length of the heavy fermion, $2\pi/m_f$. This is almost correct; the actual calculations of quantum energies for the QED flux tube (eqs. (42) and (43) in ref. [18]) show that the proper scaling factor is in fact *half* the Compton wave-length. Thus, the physically sensible choice for v^2 is

$$v_{D=2+1}^2 = \frac{\pi}{m_f} v_{D=3+1}^2 = \frac{\pi}{2\sqrt{2}G_F m_f}. \quad (3.15)$$

For the remaining parameters, *i.e.* the masses that determine the coupling constants f , g and λ , we can directly take the values suggested by electroweak phenomenology:

$$m_f = f v_{D=3+1} = 170 \text{ GeV}, \quad \frac{g v_{D=3+1}}{\sqrt{2}} = 80 \text{ GeV} \quad \text{and} \quad 2 v_{D=3+1} \sqrt{\lambda} = 115 \text{ GeV}. \quad (3.16)$$

We have identified the heavy fermion doublet with the top/bottom pair and set m_f to the top quark mass. In our numerical studies, we have also experimented with a very heavy fermion to investigate possible decoupling scenarios.

D. The Counterterms

The counterterm coefficients c_i in (3.13) must be chosen to cancel the divergences in low-order Feynman diagrams. In $D = 2 + 1$, only the first two diagrams (with $n = 1$ and $n = 2$ insertions of the background potential $-iU$) are divergent and it is readily seen that the terms in (3.13) are sufficient to render the sum of the $n = 1, 2$ diagrams — and thus the entire vacuum polarization part E_{vac} — finite. The remaining arbitrariness in the definition of the c_i is fixed by conventional renormalization conditions (see, for instance, ref. [27]):

- a. We start by choosing the so-called *no-tadpole* condition. This ensures that neither the VEV $\langle\phi\rangle = v(0, 1)^T$ nor the perturbative fermion mass m_f receive radiative corrections. This condition determines c_3 .
- b. We fix the pole of the Higgs propagator to be at its tree level mass, M_H , with residue one. These conditions yield c_2 and c_4 .
- c. There are various choices to fix the remaining coefficient c_1 . We choose to set the *residue* of the pole of the gauge field propagator to one in unitary gauge. The *position* of that pole, *i.e.* the mass of the gauge field, M_W , is then a prediction.

The resulting counterterm coefficients c_i are listed in the Appendix. As explained under item c., the mass of the gauge fields is constrained by the other model parameters when fermion loops are included. With our choice of renormalization conditions, M_W is the solution to the implicit equation

$$\xi_W^2 = \frac{g^2 v^2}{2m_f^2} \left(1 + \frac{f^2}{\pi m_f} I_2(\xi_W)\right) + \frac{g^2}{16\pi m_f} (\xi_W^2 I_1(\xi_W) + 2\bar{I}_1(\xi_W)), \quad (3.17)$$

where $\xi_W = M_W/m_f$; the Feynman parameter integrals I_1 , \bar{I}_1 and I_2 are also given in the Appendix. If we take for g and $m_f = fv$ the values extracted from eqs. (3.15) and (3.16), we can solve eq. (3.17) numerically to obtain the fermion loop correction to the gauge boson mass. Due to the condition c. above, this mass corresponds to one- W -boson states in unitary gauge.

Of course, other renormalization conditions are possible. They correspond to finite changes in the parameters c_i which are exactly calculable and affect the counterterm contribution eq. (3.13) only. The renormalization group ensures that such re-parameterizations do not change the physical content of the model.

E. The Vacuum Polarization Energy

From eq. (3.9) the one-fermion-loop correction to the bosonic background energy is an infinite series of Feynman diagrams, which is impossible to sum in practice. Perturbative methods based on the lowest order diagrams are ineffective, since the coupling of the heavy fermion to the boson background is not naturally small. Instead, we follow the spectral approach introduced in refs. [28, 29] for an *exact* calculation of the renormalized fermion vacuum polarization. For a detailed review of this method and a list of further references, see ref. [17].

The spectral approach is based on the observation that the vacuum polarization can alternatively be characterized as a sum over the change in the zero-point energies of the fermion modes due to the background fields. The fermion modes comprise both the bound states of energy ϵ_j (with degeneracy D_j), and the scattering modes characterized by a momentum density of states. If $\Delta\rho(k)$ denotes the *change* in the density of the scattering states caused by the non-trivial background, we have the expression

$$E_{\text{vac}} = -\frac{1}{2} \sum_j D_j (|\epsilon_j| - m_f) - \frac{1}{2} \int_0^\infty dk (\sqrt{k^2 + m_f^2} - m_f) \Delta\rho(k) + E_{\text{ct}} \quad (3.18)$$

where the degeneracy factor D_j in $D = 2 + 1$ dimensions is unity if the sum over j runs from $-\infty$ to ∞ . The cancellation of the divergences in the momentum integral by conventional counterterms E_{ct} is still formal at this stage.

What makes the spectral method effective is the fundamental relation between the change in the continuum density of states and the scattering phase shifts $\delta_\ell(k)$ of the Dirac wave-functions [30]

$$\Delta\rho(k) = \frac{1}{\pi} \frac{d}{dk} \sum_\ell D_\ell \delta_\ell(k). \quad (3.19)$$

The shorthand notation ℓ will be used in the following to denote the collection of all quantum numbers (including the sign of the energy and generalized angular momentum) that characterize an individual scattering channel.

Since the Feynman series is an expansion in powers of the interaction potential eq. (3.7), the same expansion in the spectral method suggests a one-to-one correspondence between Feynman diagrams and the *Born expansion* of the phase shifts. This reasoning is essentially correct, though there is a slight subtlety associated with the string background. Ignoring this issue for a moment, we may subtract the lowest orders of the Born series from the phase shifts, and add back in *exactly* the same quantity in the form of Feynman diagrams:

$$E_{\text{vac}} = -\frac{1}{2} \sum_j D_j(|\epsilon_j| - m_f) - \frac{1}{2} \int_0^\infty \frac{dk}{\pi} (\sqrt{k^2 + m_f^2} - m_f) \frac{d}{dk} [\delta(k)]_N + \left[\sum_{i=1}^N E_{\text{FD}}^{(i)} + E_{\text{ct}} \right], \quad (3.20)$$

Here, $[\delta(k)]_N$ is a shorthand notation for the sum over all channels ℓ of the full phase shift (including the degeneracy) minus the first N terms of the respective Born series. Ref. [31] contains a careful derivation of eq. (3.20) that starts directly from the definition of the energy-momentum tensor in field theory.

All three contributions in eq. (3.20) are separately finite as the regulator is removed: The bound state is a finite sum, the momentum integral converges due to the Born subtraction, and the last piece is a conventional perturbative calculation of the N lowest order Feynman diagrams (with counterterms to implement the renormalization conditions discussed above). For the present model in $D = 2 + 1$, only the first and second order Feynman diagrams require renormalization, *i.e.* $N = 2$ is the minimal number of Born subtractions necessary for a finite calculation. The final expression for the vacuum polarization energy is thus

$$E_{\text{vac}} = -\frac{1}{2} \sum_j D_j(|\epsilon_j| - m_f) - \frac{1}{2} \int_0^\infty \frac{dk}{\pi} (\sqrt{k^2 + m_f^2} - m_f) \frac{d}{dk} [\delta(k)]_2 + E^{(1,2)} + E_{\text{ct}}^{(3,4)}. \quad (3.21)$$

The first and second order diagrams, combined with the counterterms of the same order give the finite contribution $E^{(1,2)}$. The third and fourth order diagrams are *not* divergent in $D = 2 + 1$ (and therefore left as implicit part of the momentum integral), but we still need finite counterterms $E_{\text{ct}}^{(3,4)}$ for them to enforce the correct renormalization conditions. The explicit expressions for $E^{(1,2)}$ and $E_{\text{ct}}^{(3,4)}$ can be found in the Appendix.

Let us finally discuss the subtlety associated with the Born approximation in the string background. It is due to the fact that Feynman diagram calculations require *all* field derivatives to vanish sufficiently fast as $\rho \rightarrow \infty$. This condition is not met by the vortex, which has winding and thus nonzero azimuthal derivatives at $\rho \rightarrow \infty$. In $D = 2 + 1$, only the counterterm coefficient c_3 is UV divergent while the remaining (finite) c_i serve to enforce our renormalization scheme. The counterterm multiplied by c_3 involves only $(\phi^\dagger \phi)$, so instead of doing the full Born subtraction and the corresponding diagrams, we can perform this piece of the calculation in a *fictitious* background with the same value $(\phi^\dagger \phi)$ as our initial vortex background. On the sphaleron square, we can, for example, choose the corresponding boundary point with $\xi_1 = 0$ and $\xi_2 = \pi/2$, *cf.* Sec. II B, where all gauge fields vanish and ϕ has no azimuthal dependence at $\rho \rightarrow \infty$. For this fictitious background, the subtraction/diagram part of the calculation is straightforward.

F. The Dirac Equation

The final ingredients in our computational method are the equations of motion for the fermion fields and the associated techniques used to extract the phase shifts in the boson background.

1. First-order equations

We start from the Dirac equation in $2 + 1$ dimensions, which we write in the form⁵

$$h_D \Psi_{\omega, N_\ell}(\rho, \varphi) = \omega \Psi_{\omega, N_\ell}(\rho, \varphi), \quad (3.22)$$

⁵ With four-component Dirac spinors, the same equation also holds in $D = 3 + 1$, provided that all fields are translationally invariant along the string (which we put along the z -axis) and the gauge fields have vanishing z -components. This means that the bound states and phase shifts computed in this section are also appropriate for $D = 3 + 1$ and the trivial space dimension can be managed by the interface formalism [19]. Complications arise in $D = 3 + 1$ only because the renormalization procedure is more elaborate.

The single particle Dirac operator can be read off from eq. (3.4),

$$h_D = -i\alpha^i \partial_i + \gamma^0 f (P_R \Phi + P_L \Phi^\dagger) - g \alpha^i \left[Z_i Q_Z + P_L (W_i^+ T^- + W_i^- T^+) \right], \quad (3.23)$$

where $\alpha^i = \gamma^0 \gamma^i$ and $i = 1, 2$. Our vortex configurations are special cases of a class of background fields which show an angular dependence similar to the Nielson–Olesen vortex of winding number n ,

$$\phi_0 \propto e^{in\varphi}, \quad \phi_+ \propto 1, \quad \vec{W}^3 \propto \hat{\varphi}, \quad \vec{W}^+ = (\vec{W}^-)^* \propto e^{-in\varphi} \hat{\varphi}, \quad (3.24)$$

This class of configurations exhibits a symmetry: Since the heavy fermion doublet is degenerate, the operator

$$K = L_3 + S_3 - nT_3\gamma_5 \quad (3.25)$$

commutes with the Hamiltonian h_D . Its eigenvalues $N_\ell = \ell + \frac{1}{2} + \frac{n}{2}$ may therefore be used to label the fermion modes and channels in a vortex background of the specified form.

As explained earlier, we want to keep our computation as close as possible to the $D = 3 + 1$ case, and therefore employ Dirac 4-spinors even in $D = 2 + 1$. This redundancy implies the existence of a matrix α^3 with the property $\{\alpha^3, h_D\} = 0$. For every eigenspinor Ψ of the Dirac operator with eigenvalue ω , there exists an corresponding state $\alpha^3 \Psi$ with eigenvalue $-\omega$, and the spectrum of h_D is manifestly symmetric about zero.

For the actual calculation we choose the chiral representation of the Dirac matrices (with $\gamma^5 = \text{diag}(-1, -1, 1, 1)$ and $S_3 = \text{diag}(1, -1, 1, -1)/2$) and parameterize the eigenspinors by eight functions y_1, \dots, y_8 that only depend on the radial coordinate ρ ,

$$\Psi_{\omega, N_\ell}(\rho, \varphi) = \begin{pmatrix} y_5 e^{i\ell\varphi} |\frac{1}{2}\rangle + y_7 e^{i(\ell+n)\varphi} |-\frac{1}{2}\rangle \\ iy_6 e^{i(\ell+1)\varphi} |\frac{1}{2}\rangle + iy_8 e^{i(\ell+n+1)\varphi} |-\frac{1}{2}\rangle \\ y_1 e^{i(\ell+n)\varphi} |\frac{1}{2}\rangle + y_3 e^{i\ell\varphi} |-\frac{1}{2}\rangle \\ iy_2 e^{i(\ell+n+1)\varphi} |\frac{1}{2}\rangle + iy_4 e^{i(\ell+1)\varphi} |-\frac{1}{2}\rangle \end{pmatrix} \quad (3.26)$$

The kets in this expression are eigenvectors of $T^3 = \tau^3/2$. We may re-cast the $D = 2 + 1$ Dirac Hamiltonian in 2×2 block form as

$$h_D = \begin{pmatrix} h_{11} & h_{12} \\ h_{21} & h_{22} \end{pmatrix}. \quad (3.27)$$

In the chiral representation of the Dirac matrices (and in temporal gauge) these 2×2 blocks have a very simple dependence on the background fields,

$$\begin{aligned} h_{11} &= i\sigma_i \partial_i + g \sigma_i \{Z_i T^3 + W_i^+ T^- + W_i^- T^+\}, \\ h_{22} &= -i\sigma_i \partial_i, \\ h_{12} &= f\Phi, \\ h_{21} &= f\Phi^\dagger. \end{aligned} \quad (3.28)$$

2. Second-order Equations

To extract the scattering data, the second order form of the equations of motion is more appropriate. We find these by substituting the Dirac operator eq. (3.27) into the first order form eq. (3.22) which eliminates half of the field components (while doubling the order of the differential equation). We choose to eliminate the left-handed fields, which are the upper components in the chiral representation. The resulting equation of motion for the right-handed (lower) Weyl spinor Ψ_R reads

$$h_{21} [(h_{11} - \omega)h_{21}^{-1}(h_{22} - \omega) - h_{12}] \Psi_R = 0. \quad (3.29)$$

These are two complex second-order equations for the two complex components of Ψ_R . Upon inserting the parameterization eq. (3.26), we obtain four second-order equations for the radial functions appearing in Ψ_R ,

$$\sum_{j=1}^4 \left\{ \mathcal{D}(\rho) + \mathcal{N}(\rho) \frac{d}{d\rho} + \mathcal{M}(\rho) \right\}_{ij} y_j(\rho) = 0. \quad (3.30)$$

with $k^2 = \omega^2 - m_f^2$. The kinetic operator \mathcal{D} contains a radial piece from the 2D Laplacian, as well as a generalized centrifugal barrier \mathcal{O} ,

$$\mathcal{D}(\rho) = \mathbb{1} \left(\frac{d^2}{d\rho^2} + \frac{1}{\rho} \frac{d}{d\rho} + k^2 \right) - \frac{1}{\rho^2} \mathcal{O}, \quad \mathcal{O} = \text{diag} [(\ell+n)^2, (\ell+n+1)^2, \ell^2, (\ell+1)^2]. \quad (3.31)$$

The matrices $\mathcal{N}(\rho)$ and $\mathcal{M}(\rho)$ contain the bosonic background potential. The explicit form of the matrix elements is rather lengthy, particularly for the non-trivial background *ansätze* in our numerical treatment; we refrain from presenting them in any detail. At large radii $\rho \rightarrow \infty$, the background potential vanishes and $\mathcal{N}(\rho) \rightarrow 0$ as well as $\mathcal{M}(\rho) \rightarrow 0$, and the four differential equations decouple.

The bound state energies ϵ_j can be computed directly from eq. (3.22) by shooting for normalizable solutions that are regular at the origin and decay exponentially at large radii $\rho \rightarrow \infty$. By contrast, the phase shifts, which are extracted from eq. (3.30), require a few more manipulations to put the calculation in a manageable form.

We have a four-channel scattering problem that can be treated in the usual fashion: The full eigenspace to a given energy ω is decomposed into channels labeled by the integral angular momentum ℓ . In each such channel, we have four independent solutions $\mathbf{y}(\rho)$ to eq. (3.30), which we may combine in the *rows* of a matrix \mathcal{Y} . Thus, $\mathcal{Y}_{ij}(\rho, k)$ is the radial function $y_j(\rho)$ in the i^{th} linearly independent solution at a fixed momentum k and channel number ℓ (we suppress ℓ in the following).

Let us analyze the free case $\mathcal{M} = \mathcal{N} = 0$ first. The solutions with outgoing spherical wave boundary conditions at $\rho \rightarrow \infty$, are $\mathcal{Y}(\rho, k) = \mathcal{H}(k\rho)$ with

$$\mathcal{H}(x) = \text{diag} [h_{|\ell+n|}^{(1)}(x), h_{|\ell+n+1|}^{(1)}(x), h_{|\ell|}^{(1)}(x), h_{|\ell+1|}^{(1)}(x)] \quad (3.32)$$

given explicitly in terms of Hankel functions. Similarly, for $\mathcal{M}, \mathcal{N} \neq 0$, the scattering states $\mathbf{y}(\rho)$ are solutions of the fully interacting equations of motion (3.30), which tend to specific free outgoing waves of the same energy at $\rho \rightarrow \infty$. Combining them in a (4×4) matrix as before, we may split off the asymptotic form by the ansatz $\mathcal{Y}(\rho, k) = \mathcal{F}(k, \rho) \cdot \mathcal{H}(k\rho)$. Inserting into eq. (3.30), we find the differential equation for the Jost-like matrix $\mathcal{F}(k, \rho)$,

$$\mathcal{F}'' + \frac{1}{\rho} \mathcal{F}' + 2\mathcal{F}' \mathcal{L}' + \frac{1}{\rho^2} [\mathcal{F}, \mathcal{O}] + \mathcal{N}(\mathcal{F}' + \mathcal{F} \mathcal{L}') + \mathcal{M} \mathcal{F} = 0, \quad (3.33)$$

where $\mathcal{L}(k\rho) \equiv \ln \mathcal{H}(k\rho)$ and primes denote derivatives with respect to the radial coordinate. If we impose the boundary conditions

$$\mathcal{F}(k, \rho) \rightarrow \mathbb{1}, \quad \mathcal{F}'(k, \rho) \rightarrow 0$$

at $\rho \rightarrow \infty$, the corresponding solution matrix $\mathcal{Y}(\rho, k) = \mathcal{F}(k, \rho) \cdot \mathcal{H}(k\rho)$ clearly describes outgoing spherical waves. What is unusual about the string background is that the matrices \mathcal{M} and \mathcal{N} may actually be complex. As a consequence, the conjugated matrix \mathcal{Y}^* does *not* describe *incoming* spherical waves; in fact, it is not even a solution of the equations of motion. Instead, the scattering states corresponding to incoming waves, which we denote by $\overline{\mathcal{Y}}$ in the following, must be computed separately by an appropriate change in the Hankel functions $\mathcal{H} \rightarrow \overline{\mathcal{H}}$. The standard scattering analysis now proceeds as usual with \mathcal{Y}^* replaced by $\overline{\mathcal{Y}}$.⁶

The scattering wavefunction can now be written as

$$\mathcal{Y}_{\text{sc}}(\rho) = -\overline{\mathcal{Y}}(\rho) + \mathcal{Y}(\rho) \cdot \mathcal{S}(k). \quad (3.34)$$

Requiring that $\mathcal{Y}_{\text{sc}}(\rho)$ be regular at the origin yields a relation for the scattering matrix,

$$\mathcal{S}(k) = \lim_{\rho \rightarrow 0} \mathcal{Y}^{-1}(\rho) \cdot \overline{\mathcal{Y}}(\rho) = \lim_{\rho \rightarrow 0} \mathcal{H}^{-1}(k\rho) \cdot \mathcal{F}^{-1}(k, \rho) \cdot \overline{\mathcal{F}}(k, \rho) \cdot \overline{\mathcal{H}}(k\rho). \quad (3.35)$$

For the spectral method (3.21), we need the sum of the eigenphase shifts obtained from \mathcal{S} ,

$$\delta(k) = \frac{1}{2i} \text{Tr} \ln \mathcal{S}(k) = \frac{1}{2i} \lim_{\rho \rightarrow 0} \text{Tr} \ln (\mathcal{F}^{-1}(k, \rho) \cdot \overline{\mathcal{F}}(k, \rho)). \quad (3.36)$$

⁶ Alternatively, we could rewrite the complex (4×4) problem as a real (8×8) problem. The phase shifts – or more precisely the sum of eigenphaseshifts in each channel – extracted in this way are exactly *twice* as large as the ones from the initial (4×4) problem. This statement is obvious in the case that the matrices \mathcal{M} and \mathcal{N} are real, and we have checked it numerically in other cases.

It should be noted that the fermion flux in the chiral basis is not orthonormal and the matrix \mathcal{S} is hence not unitary. However, the physical scattering matrix can be obtained from \mathcal{S} by a change of basis and proper normalization. Both manipulations do not alter the sum of eigenphase shifts, which is the relevant quantity here.

In our numerical calculations, we do not use eq. (3.36) directly; instead we set

$$\delta(k, \rho) \equiv \frac{1}{2i} \text{Tr} \ln (\mathcal{F}^{-1}(k, \rho) \cdot \overline{\mathcal{F}}(k, \rho)) , \quad (3.37)$$

such that $\delta(k) = \delta(k, 0)$. To compute this function, we integrate the differential equation

$$\frac{\partial \delta(k, \rho)}{\partial \rho} = -\frac{1}{2i} \text{Tr} \left[\mathcal{F}' \cdot \mathcal{F}^{-1} - \overline{\mathcal{F}}' \cdot \overline{\mathcal{F}}^{-1} \right] , \quad \lim_{\rho \rightarrow \infty} \delta(k, \rho) = 0 \quad (3.38)$$

along with the system for \mathcal{F} and $\overline{\mathcal{F}}$ from $\rho = \infty$ to 0. This procedure results in a smooth function of both ρ and k , which avoids ambiguous jumps of (multiples of) π and allows to take the limit $\rho \rightarrow 0$ easily.

Notice finally that channels which involve Hankel functions of order $\ell = 0$ are afflicted by a further numerical subtlety. Eq. (3.36) essentially requires to separate the regular and irregular pieces as $\rho \rightarrow 0$. For $\ell = 0$ this amounts to distinguishing a logarithmic behavior from a constant, which is difficult to handle numerically. In this case, we switch to a radial function analogous to $\delta(k, \rho)$, which is defined in terms of the radial *derivatives* of $\mathcal{F}(k, \rho)$ and $\mathcal{L}(k, \rho)$. We have checked the numerical stability of this treatment thoroughly.

G. Derivative expansions

To check our numerical results, it is helpful to have analytic approximations to the vacuum polarization energy. The lowest orders of a *perturbative* expansion are already contained in our main formula eq. (3.21); to check the phase shift piece of the calculation, we would therefore have to compute (many) higher order diagrams, which is very cumbersome. A better strategy is to employ a *derivative expansion* which is expected to work well for reasonably broad background profiles.

The leading order of the gradient expansion is the effective potential, V_{eff} , which contains no derivatives of the boson background fields. Together with gauge invariance, this restriction rules out any dependence on the gauge fields, so V_{eff} is a functional of the Higgs field alone. In $D = 2 + 1$ dimensions, V_{eff} is formally given by

$$- \int d^3x V_{\text{eff}}[\phi] = -i \text{Tr} \ln (i\partial - f\Phi_5) \quad (3.39)$$

for a *constant* background $\Phi_5 = \Phi P_L + \Phi^\dagger P_R$, cf. eq. (3.5). The functional trace is divergent and needs to be renormalized by adding the same counterterms as were determined in section III D. To get definite expressions, we employ dimensional regularization and write

$$- \int d^3x \frac{\partial V_{\text{eff}}[\phi]}{\partial f} = (-i)f \text{Tr} \left\{ \left[\partial^2 + f\Phi_5\Phi_5^\dagger \right]^{-1} \Phi_5\Phi_5^\dagger \right\} \rightarrow i f \int d^Dx \int \frac{d^Dk}{(2\pi)^D} \text{tr} \left\{ \left[k^2 - f\Phi_5\Phi_5^\dagger \right]^{-1} \Phi_5\Phi_5^\dagger \right\} . \quad (3.40)$$

The analytic continuation of the integral on the rhs to $D = 3$ is finite, so that one would expect to need no renormalization at all. However, the integral is manifestly convergent only in $D = 1$ and the continuation to $D = 3$ is unambiguous only if the divergence in the even dimension $D = 2$ is canceled by counterterms. Only the sum of the integral and counterterm is analytic in the range $D = 1$ to $D = 3$ and we *must* renormalize for all $D \geq 2$. Furthermore, we need to impose renormalization conditions that match our previous scheme if we want to compare the results of the derivative expansion with the spectral method. Upon integrating eq. (3.40) with respect to the Yukawa coupling and fixing the integration constant via the normalization $V_{\text{eff}}[v] = 0$, we obtain the result

$$V_{\text{eff}}[\phi] = \frac{2}{3\pi} f^3 \left[(\phi^\dagger \phi)^{3/2} - v^3 \right] - \frac{vf^3}{\pi} \left[\phi^\dagger \phi - v^2 \right] - c_4 \left[\phi^\dagger \phi - v^2 \right]^2 . \quad (3.41)$$

The explicit expression for the counterterm coefficient c_4 is rather lengthy; it can be read off from eq. (A2) in the appendix. Notice that the effective potential is minimized for configurations with $\phi^\dagger \phi = v^2$; this is, of course, a direct consequence of our *no-tadpole* renormalization condition.

For the next-to-leading order in the derivative expansion, there are well-known techniques [32, 33] that apply straightforwardly in the case of a pure Higgs background. On the sphaleron square, these are the configurations with

$\xi_1 = 0$. We will see in the next section that such backgrounds play a prominent role. The result for the effective Lagrangian is

$$\mathcal{L}_{\text{eff}}^{(2)} = \frac{f}{16\pi} \left\{ (\phi^\dagger \phi)^{-1/2} (\partial_\mu \phi)^\dagger (\partial^\mu \phi) - \frac{1}{3} (\phi^\dagger \phi)^{-3/2} \partial_\mu (\phi^\dagger \phi) \partial^\mu (\phi^\dagger \phi) \right\}, \quad (3.42)$$

where the superscript indicates that this term contains two derivatives of the Higgs background. Again, the expression eq. (3.42) is ultra-violet finite in $D = 2 + 1$, but we need to add the two derivative counterterms, eq. (3.10), to match our previous renormalization conditions.

In a gauge invariant expansion, the leading order effect of the gauge bosons is to turn the ordinary derivatives in eq. (3.42) into *covariant derivatives* of the form eq. (2.5).⁷ Inserting the explicit form eq. (2.21) of the static vortex background, our final expression for the derivative expansion of the vacuum polarization energy is

$$\begin{aligned} E_{\text{vac}} \approx 2m_f \pi \int_0^\infty x dx \left\{ \frac{2}{3\pi} \left[(f_H^2 + f_P^2)^{3/2} - 1 \right] + \frac{1}{\pi} (1 - f_H^2 - f_P^2) - \frac{v^4 c_4}{m_f^3} (1 - f_H^2 - f_P^2)^2 \right. \\ \left. + \left[\frac{1}{16\pi} (f_H^2 + f_P^2)^{-1/2} + \frac{m_f c_2}{f^2} \right] \left[f_H'^2 + f_P'^2 + \frac{n^2}{x^2} (f_H^2 (1 - f_G^2) + f_P^2 f_G^2) \sin^2 \xi_1 \right] \right. \\ \left. + \frac{1}{12\pi} (f_H^2 + f_P^2)^{-3/2} (f_H f_H' + f_H f_H')^2 \right\}, \end{aligned} \quad (3.43)$$

where primes denote derivatives with respect to the dimensionless variable $x = m_f \rho$.

IV. NUMERICAL STUDIES

Our goal is to find a spatially varying configuration of the boson fields that is energetically favored over the trivial vacuum configuration with the same fermion number. To this end we scan the energy surface with respect to variational parameters in specific *ansätze* for the background profiles. The comparison requires, of course, that both the trivial and non-trivial configuration have identical fermion numbers. As discussed at the beginning of section III, the vortex background acquires its fermion number by occupying the N_f lowest fermion bound states; its energy must then be compared to the trivial configuration with energy $N_f m_f$, cf. eq. (3.3). These considerations become slightly more complicated if internal degrees of freedom (*e.g.* color) are included, as is discussed in more detail below.

Our variational ansatz is discussed in detail in the next subsection. Altogether, it involves five parameters; even though this number is already numerically expensive to be scanned, it is definitely not exhaustive, so stable configurations can still exist that we have not found. However, if we find an energetically favored object, expanding the ansatz will only improve on this result. We will begin by exploring the parameter dependence of the various contributions to the total energy and then turn to the search for bound objects with large fermion numbers.

A. Explicit profiles

Unless stated otherwise, we shall employ the following *ansätze* for the radial profiles in the string background:

$$f_H = 1 - e^{-\rho/w_H}, \quad f_G = 1 - e^{-(\rho/w_G)^2} \quad \text{and} \quad f_P = a_P e^{-\rho/w_P}. \quad (4.1)$$

The constants w_H , w_G and a_P , together with ξ_1 , eq. (2.24), are variational parameters that characterize the background fields, which we will adjust to minimize the energy functional $E_{\text{eff}}^{(N_f)}$, eq. (3.2). The profile functions f_H and f_G defined above are constructed such that the classical energy is always finite, regardless of the values chosen for the variational parameters. Near the origin, these radial functions behave as $f_H \propto \rho$ and $f_G \propto \rho^2$ while for large ρ both profile functions tend to unity. We certainly could introduce additional degrees of freedom subject to the boundary conditions. Introducing additional parameters for the amplitudes of the exponential functions in f_H and f_G violates this requirement of finite classical energy, however, and hence we refrain from doing so.

⁷ There are various approaches to counting derivatives in a covariant expansion; some of these schemes expand in the gradients of the magnetic field, so the leading term will contain \mathbf{B} (and hence the derivatives of the gauge field) at all orders. For our purposes, the simple expression (3.43) is sufficient.

B. Classical Energy

We first discuss the results for the classical energy E_{cl} . We consider the W -string on the sphaleron square, eq. (2.24), with the classical energy

$$E_{\text{cl}} = 2\pi \int_0^\infty \rho d\rho \mathcal{E}_{\text{cl}}. \quad (4.2)$$

The classical energy density, \mathcal{E}_{cl} , is given by eq. (2.23) plus the contribution of the additional scalar field f_P as given in eq. (2.26). We always assume unit winding $n = 1$.

We first discuss the case for physical (standard model) parameters augmented by the choice of the VEV in $D = 2 + 1$ dimensions, eq. (3.15). In what follows all data are measured in units of m_f or its inverse. For the classical energy, we observe a strong dependence on the angle ξ_1 , which parameterizes the interpolation between the W -string and a purely scalar configuration with the same Higgs profile $|\phi|^2$.

Even though the mixing angle ξ_1 is one of our variational parameters, it is fruitful to discuss the energy functional for various *fixed* values of ξ_1 and attempt to minimize E_{cl} in the space of the remaining variational parameters. Note, however, that minimization of E_{cl} is not the main goal of our investigations. For small ξ_1 the gauge field contributions are suppressed and the minimal value for E_{cl} is obtained for small Higgs field extensions. In the extreme case of no gauge fields ($\xi_1 = 0$) we expect $E_{\text{cl}} \approx 6$ as $w_H \rightarrow 0$ and $a_P = 0$ from the scaling properties of the derivative terms in $\int \rho d\rho \mathcal{E}_{\text{cl}}$, cf. eq. (2.23). For $\xi_1 = 0.05\pi$, $w_H = 1.1$, $w_P = 2$ and $a_P = 0.1$ we find $E_{\text{cl}} \approx 9$. The classical energy essentially increases quadratically with w_H . On the other hand, the dependence on w_P appears to be weak, even for sizable $a_P \geq 0.5$. For moderate $\xi_1 \approx \pi/4$, the classical energy is again minimized by narrow Higgs fields while the gauge fields tend towards intermediate sizes ($w_G \approx 3$). However, the value for the (minimal) classical energy at fixed $\xi_1 \sim \pi/4$ is increased by about a factor 2 as compared to $\xi_1 \sim 0$. In the regime of its maximal value $\xi_1 \sim \pi/2$, the (minimal) classical energy is even further increased to about 30. Again, in this case the minimal value occurs at non-zero extension of the Higgs field $w_H \approx 3$. When we study the effect of the additional contribution from f_P , we also see that the minimal classical energy occurs at small ξ_1 and it does not vary much in the range $a_P \in [0.1, 0.5]$. Beyond that regime the classical energy starts rising linearly with a_P .

We find it worth mentioning that the configuration we have investigated in detail with the lowest classical energy does not have exactly $\xi_1 = 0$, where the gauge field part in the background configuration vanishes identically, but rather $\xi_1 = 0.05\pi$. As we have seen before, even for this small value of ξ_1 the gauge field energy is of a noticeable size. We note, however, that $\xi_1 = 0$ is problematic for the numerical investigation as will be discussed further below, cf. footnote 9.

To some extent the situation is different for large fermion masses. Even though the classical energy does not explicitly depend on m_f , this quantity enters via the VEV in $D = 2 + 1$ dimensions, eq. (3.15), and also affects the numerical result for E_{cl} as it sets the overall energy scale⁸. We have numerically studied the case with $m_f = 1.5\text{GeV}$. For small ξ_1 the classical energy is also small, *i.e.* for $\xi_1 \leq 0.1$ we find $E_{\text{cl}} \lesssim 0.4$. The numerical values for the classical energy seem quite insensitive to the shape of the Higgs field as the coupling via the VEV is drastically decreased. Of course, for small ξ_1 the dependence on w_G is again mitigated. This changes for moderate values of ξ_1 . For $\xi_1 \approx 0.5$ we have varied $w_G \in [1.5, 5.5]$. In that range E_{cl} strongly varies between approximately 2 and 25 with the smallest result obtained for the largest width w_G . On the other hand, the dependences on the Higgs field variational parameters is soft. We observe a similar situation for ξ_1 in the vicinity of $\pi/2$, when the relative contribution from the gauge fields is maximal. However, the range along which E_{cl} changes is even bigger. For small w_G (~ 1.5), it may be as big as 50 while it reaches values close to one for very large widths of the gauge fields $w_G \approx 12$. We do not thoroughly study such configurations because in these cases the computation of the vacuum polarization energy is numerically very costly. Minimization of the classical energy requires a suppression of the gauge boson contribution (small ξ_1) and/or a sizable extension of these fields. In the following sections we will study the behavior of the fermion vacuum energy under these conditions. In particular, we will study the question of whether or not the energy gain due to the emergence of a fermion zero mode at $\xi_1 = \pi/2$ can compensate for the increase of the classical energy. The energy gain per occupied zero mode is unity and thus we expect that we need a large number of fermions (twenty or so) to break even, unless something unexpected happens to the vacuum polarization energy.

As mentioned above, the classical energy does not vanish for the limiting case of our variational parameters in which ξ_1 , w_H and a_P are all zero. The corresponding classical energy $E_{\text{cl}} \sim 6$ is the minimal value that can be

⁸ If one re-expresses the classical energy by replacing couplings by physical masses and the Fermi coupling and takes into account that the energy is measured in units of m_f it is obvious that the Higgs field contribution to the energy is suppressed relative to gauge field contribution when m_f gets large.

accommodated by our parameterization of the fields. For this configuration, we expect the fermion spectrum to be that of the trivial vacuum, hence there appears to be a minimal energy threshold that must be overcome by finite size background fields.

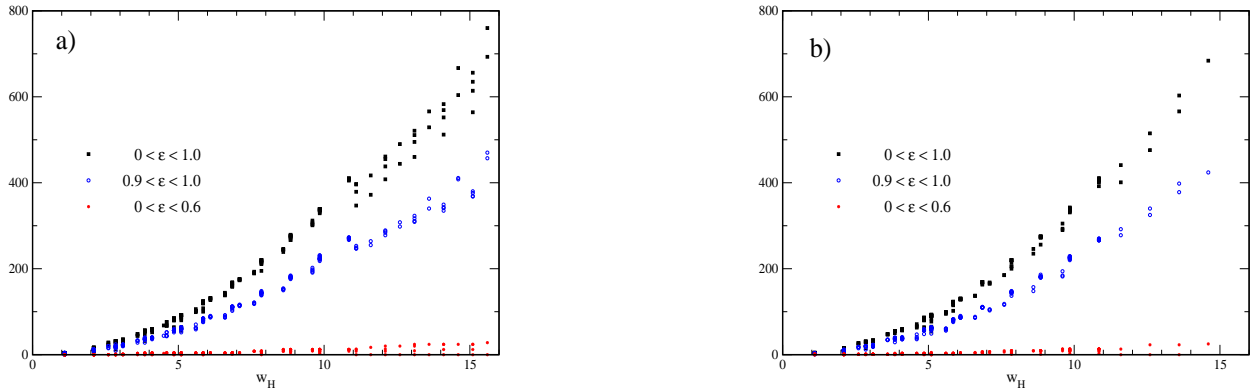
C. Bound States

Central to our analysis are the bound states of the W - and Z -strings. For $\xi_1 = \frac{\pi}{2}$ and $\phi_+ = 0$, an exact zero mode exists. Contrary to early expectations, it does not stabilize the Z -string configuration against ϕ_+ condensation once effects of the fermion determinant are taken into account, as was shown in the perturbative analysis of [4]. By taking the whole bound state spectrum into account we find something unexpected. In the background of rather wide strings (several Compton wave lengths of the fermion) we find a very large number of bound states. Because of this large number of bound states (both spread over a lot of angular momentum channels and in individual channels) the properties of individual states like the zero mode are a lot less important than previously thought. This result provides an important reason for why the purely scalar configurations are favored over the configurations containing gauge fields. For the purely scalar configurations the lowest-lying states are less strongly bound, however, and contrary to expectations from potential theory in quantum mechanics, many more bound states exist than for those configurations that generate strongly bound states. Thus the decrease of binding of the lowest-lying states makes only a small destabilizing contribution. But the price in classical energy to pay for gauge field configurations is rather high, as we have already discussed. Hence it can be advantageous to switch them off.

Before discussing the numerical results quantitatively we would like to introduce criteria for their accuracy. Numerically we find the bound states via a shooting method, in which we determine the number of bound states in each channel by Levinson's theorem. If our numerical precision is not high enough, the shooting method will miss bound states that are very close to threshold⁹. Since each state contributes to the total energy only through its binding energy, these states are relatively unimportant. Therefore it is more efficient to construct an accuracy criterion from that observation and reject those computations that do not satisfy that criterion. Let p_ℓ be the number of missed bound states and ω_ℓ be the largest bound state energy that we observed in the channel with angular momentum ℓ . From eq. (3.21) an upper limit for the numerical error in the vacuum energy is then

$$\Delta E_{\text{vac}} = \frac{1}{2} \sum_{\ell=-\infty}^{\infty} p_\ell (m_f - \omega_\ell) , \quad (4.3)$$

and we reject any computation for a given set of variational parameters that exceeded ΔE_{vac} by a prescribed value, which we generally take as 5% of the vacuum polarization energy, defined in eq. (3.21) with $D_j = 1$. Most of the rejected calculations are characterized by very small ξ_1 .



⁹ Another problem is that a shooting algorithm might miss states in pairs if they are degenerate in energy. Such a degeneracy actually occurs for $\xi_1 = 0$ because the CP symmetry is enhanced to an individual C and P symmetry. We counter this problem by avoiding the special case $\xi_1 = 0$.

FIG. 1: The number of bound states as function of the width w_H of the Higgs field for two different values of the mixing angle: $\xi_1 = 0.1 \times \pi/2$ (a) and $\xi_1 = \pi/2$ (b). We distinguish between strongly ($0 < \epsilon < 0.6$) and loosely ($0.9 < \epsilon < 1.0$) bound states. The entry $0 < \epsilon < 1.0$ obviously gives the total number of bound states. The towers in each entry show results that originate from various values of those variational parameters that are neither held fixed nor are shown along the abscissa.

In figure 1 we display the number of bound states as a function of the width parameter w_H . There are n_ℓ bound states in each orbital momentum channel and we display $\sum_\ell n_\ell$. First of all we see that the number of bound states strongly increases roughly quadratically with the width of the Higgs field. The number of bound states increases only gradually with increased coupling to the gauge fields as measured by ξ_1 , because the main reason for the appearance of these bound states is that a Higgs field with $|\Phi| < |\langle\Phi\rangle|$ produces an attractive potential for the fermions, since $f|\Phi|$ is the effective fermion mass. The number of strongly bound states also increases only gradually with ξ_1 , which is somewhat surprising since we have a zero mode for $\xi_1 = \pi/2$ and $a_P = 0$.¹⁰ However, it is not generally accompanied by additional strongly bound states.

This bound state structure suggests that the regime with small coupling to the gauge bosons ($\xi_1 \sim 0$) might be of particular interest in our analysis. We consider the bound state contribution to the vacuum energy

$$E_B = \frac{1}{2} \sum_{\text{b.s.}} (m_f - |\epsilon_i|) \quad (4.4)$$

and in figure 2 we display E_B as function of w_H and ξ_1 . We see that E_B increases with w_H approximately quadratically, while the dependence of E_B on the other variational parameters is weaker. As an example we also show E_B as a function of ξ_1 in figure 2b). Even though E_B is large for some of the configurations in the vicinity of $\xi = \frac{\pi}{2}$ the

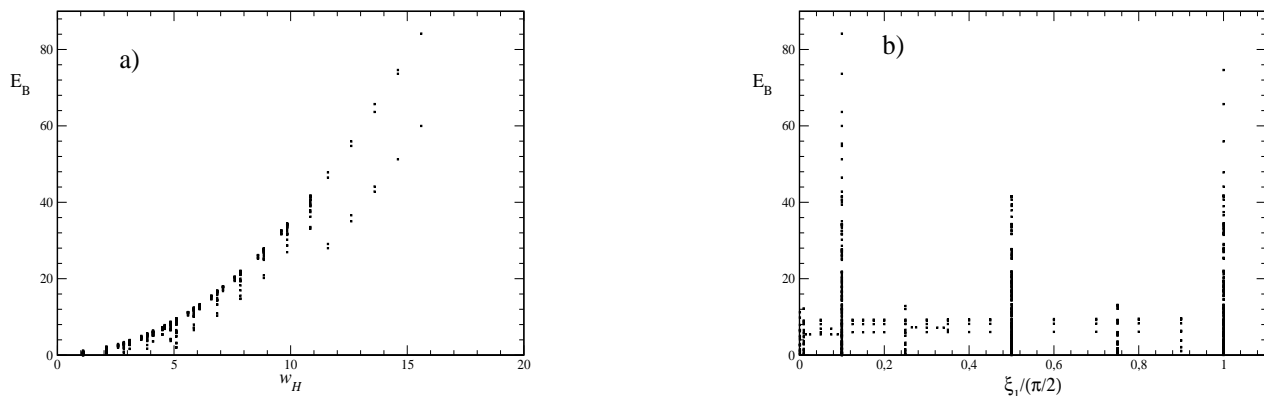


FIG. 2: The bound state contribution, E_B to the vacuum polarization energy as a function of the variational parameters a) w_H and b) ξ_1 that are defined in eqs. (2.24) and (4.1). The towers in each entry show results that originate from various values of those variational parameters that are not shown along the abscissa. It should be emphasized here - especially with regards to panel b) - that our coverage of parameter space has not been uniform. For a large range of widths, e.g., computations have only been performed for $\xi_1 = 0.1, 0.5, 0.9$. Hence one may deduce from panel b) that the range of energies is very similar for $\xi_1 = 0.1$ and $\xi_1 = 0.9$, but not that the range of energy values at $\xi_1 = 0.2$ is much smaller than for $\xi_1 = 0.1$ (in units of $\pi/2$).

maximal values are found for small ξ_1 . Since the classical energy grows with ξ_1 , it is unlikely to find stable objects in the region of large ξ_1 , *i.e.* for W dominated string configurations; rather pure Higgs configurations seem to be favored.

D. Vacuum Polarization Energy

We now turn to the discussion of numerical results for the vacuum polarization energy, E_{vac} , which we compute according to eq. (3.21). We have accumulated data for about 1000 sets of variational parameters. Our results are

¹⁰ We did not consider a configuration with $\xi_1 = \pi/2$, $w_H = 14.8$ and small a_P . Thus the $w_H = 14.8$ entry in figure 1b) misses a strongly bound state.

displayed in figure 3 for the physical value of the top quark mass $m_f = 170\text{GeV}$.

We note for some configurations the renormalized vacuum energy is negative and can provide some energy gain to the system. The maximal gain is achieved for moderate extensions of the Higgs field $w_H, w_P \sim 3 \dots 5$ while E_{vac} quickly increases when these extensions grow even further. As figure 3c) indicates, the most favored value of the gauge boson field extension is about $w_G \sim 3$. Both of these regions could also lead to a small classical energy. On the other hand we do not observe a strong dependence of E_{vac} on the angle ξ_1 cf. figure 3d). That is, the vacuum polarization part of the energy is *not* capable of overcoming the strong drift towards the Higgs dominated configuration ($\xi_1 = 0$) caused by E_{cl} . In addition, we observe that minimization of the vacuum energy induces a charged Higgs field, *i.e.* E_{vac} is minimized by $a_P \neq 0$ as shown in figure 3e).

In all we find that the energy gain from E_{vac} is only of order $-m_f$. The lowest value that we observed is $E_{\text{vac}} = -0.33m_f$ for $w_H = 5.1$, $w_P = 5.0$, $w_G = 5.5$, $a_P = 1.9$ and $\xi_1 = 0.1 \times (\pi/2)$, which is essentially a Higgs background configuration. So this energy gain alone is not sufficient to stabilize the string, but we can still populate fermion levels along the string to construct a stable object.

E. Gradient Expansion

We have already introduced the gradient (or derivative) expansion approximation as a method of checking our numerical results. In figure 4 we display the comparison of the full result, E_{vac} , which we compute according to eq. (3.20), and the gradient expansion approximation, as discussed in eq. (3.43). We display these data at the same scale as the various pieces that contribute to E_{vac} to show that the sizable cancellations that occur among these piece are necessary to accomplish the agreement with the gradient expansion approximation. In particular the case $a_P \geq 0.8$ shows that changes in the bound state contributions E_{bs} are compensated by a corresponding change in the (renormalized) Feynman diagram contribution, E_{FD} . Naïvely we expect compensations between the bound state and phase shift contributions as a reflection of Levinson's theorem. However, the Born subtractions relocate substantial pieces of the phase shift contribution into the Feynman diagrams. We only show the results as functions of the width of the Higgs field, w_H , because the dependence of the subtracted phase shift contribution E_δ on variational parameters other than w_H is negligible. Some small discrepancy between the E_{vac} and E_{DerExp} occurs at small ξ_1 because of the numerical problems we encounter in finding very weakly bound states in that case. However, this is not too worrisome because we can easily extrapolate from the region $\xi_1 \geq 0.01$.

F. Stabilization with Populating Levels

We have seen that many fermion bound states emerge for the background string configuration. We may populate these levels to describe an object with fermion number $N_f N_C$ and effective energy

$$E_{\text{eff}}^{(N_f)} = N_C \sum_{i=1}^{N_f} \epsilon_i + N_C E_{\text{vac}} + E_{\text{cl}}, \quad (4.5)$$

where the sum over the bound states is such the N_f lowest energy modes are included. The corresponding binding energy is

$$B^{(N_f)} = E_{\text{eff}}^{(N_f)} - N_C N_f m_f = N_C \sum_{i=1}^{N_f} (\epsilon_i - m_f) + N_C E_{\text{vac}} + E_{\text{cl}}. \quad (4.6)$$

Obviously $B^{(N_f)} < 0$ indicates an energetically stable object with fermion number $N_f N_C$. If there are fewer than N_f bound levels for the configuration under consideration, we have to “occupy” scattering states at threshold, which do not contribute to the binding energy. In figure 5 we display the extremal value of the binding energy for a given number (N_f) of populated levels. That is, for a prescribed value of N_f we extract the lowest $B^{(N_f)}$ in the space of variational parameters. Bound objects exist for sufficiently large N_C . In this case $N_C \geq 8$ yields a bound object with $N_f > 20$.

For small N_C , the effective energy is dominated by E_{cl} , which in turn is minimized by small w_H . In that case there are only few bound states to be populated and $B^{(N_f)}$ is saturated once all of them are occupied. For larger N_C , the fermion contribution to the effective energy becomes more important and the minimal value is obtained at larger widths, where there are more bound states and the saturation of $B^{(N_f)}$ sets in at larger values of N_f . This behavior is also reflected in figure 5.

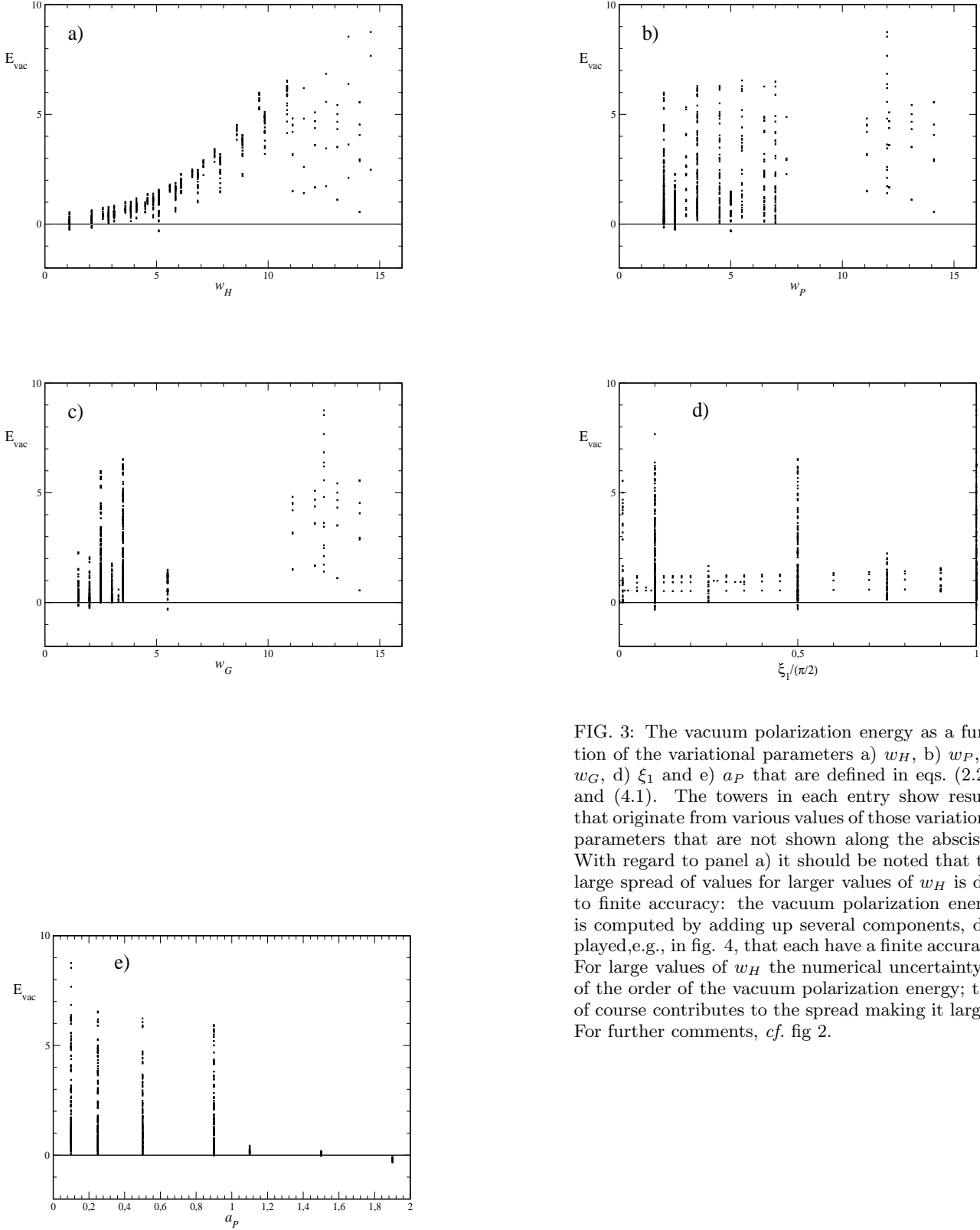


FIG. 3: The vacuum polarization energy as a function of the variational parameters a) w_H , b) w_P , c) w_G , d) ξ_1 and e) a_P that are defined in eqs. (2.24) and (4.1). The towers in each entry show results that originate from various values of those variational parameters that are not shown along the abscissa. With regard to panel a) it should be noted that the large spread of values for larger values of w_H is due to finite accuracy: the vacuum polarization energy is computed by adding up several components, displayed, e.g., in fig. 4, that each have a finite accuracy. For large values of w_H the numerical uncertainty is of the order of the vacuum polarization energy; this of course contributes to the spread making it larger. For further comments, *cf.* fig 2.

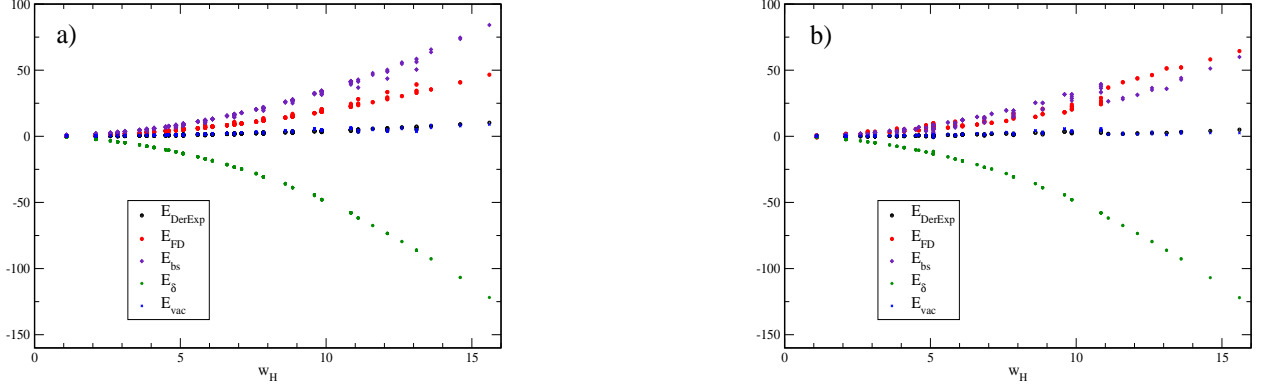


FIG. 4: Comparison of the gradient expansion results (E_{DerExp} , eq. (3.43)) with the full calculation (E_{vac} , eq. (3.20)). We also disentangle the various contributions to E_{vac} . The results are shown as functions of w_H , and we furthermore split the remaining parameters into sets with $a_P < 0.8$ (a) and $a_P \geq 0.8$ (b).

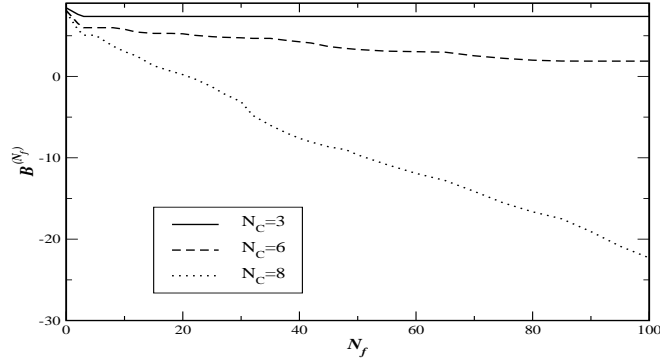


FIG. 5: The extremal (negative) binding energy, $B^{(N_f)}$ as a function of N_f , the number of populated bound state levels.

In figure 6 we display the binding energy eq. (4.6), for prescribed values of N_C and N_f , as a function of w_H to demonstrate that we indeed obtain a local minimum in the energy when the total fermion number is constrained. Again, we see that a bound object requires a large value for the number of colors.

The additional variational term a_P in eq. (2.24) is novel in the context of strings in the standard model and it is worthwhile to briefly reflect on its impact on the fermion vacuum energy. The fermion zero mode exists for $\xi_1 = \frac{\pi}{2}$ only for $a_P = 0$. In addition any non-zero value of a_P increases the effective fermion mass. Thus we expect largest binding in the small a_P regime. Indeed we find that $B^{(N_f)}$ is maximal for $a_P \rightarrow 0$. It is thus a bit surprising that a_P actually decreases the vacuum energy, *cf.* figure 3b); E_{vac} may even become negative only for sufficiently large a_P . As a consequence, at least for objects with moderate fermion numbers, the total energy does not increase with a_P despite that the energy eigenvalues of the individual fermion modes get larger. This effect is shown in figure 7.

However, for these moderate values of N_f overall binding is not yet observed. When we turn to the cases that exhibit binding, the system prefers $a_P \rightarrow 0$ because the bound states become more important as we turn up N_f . This effect is shown in figure 7.

G. Large Fermion Mass

We have seen that stable objects can be constructed by choosing unconventional parameters. In particular, increasing the number of fermion degrees of freedom helps to bind objects with large fermion numbers, since it suppresses

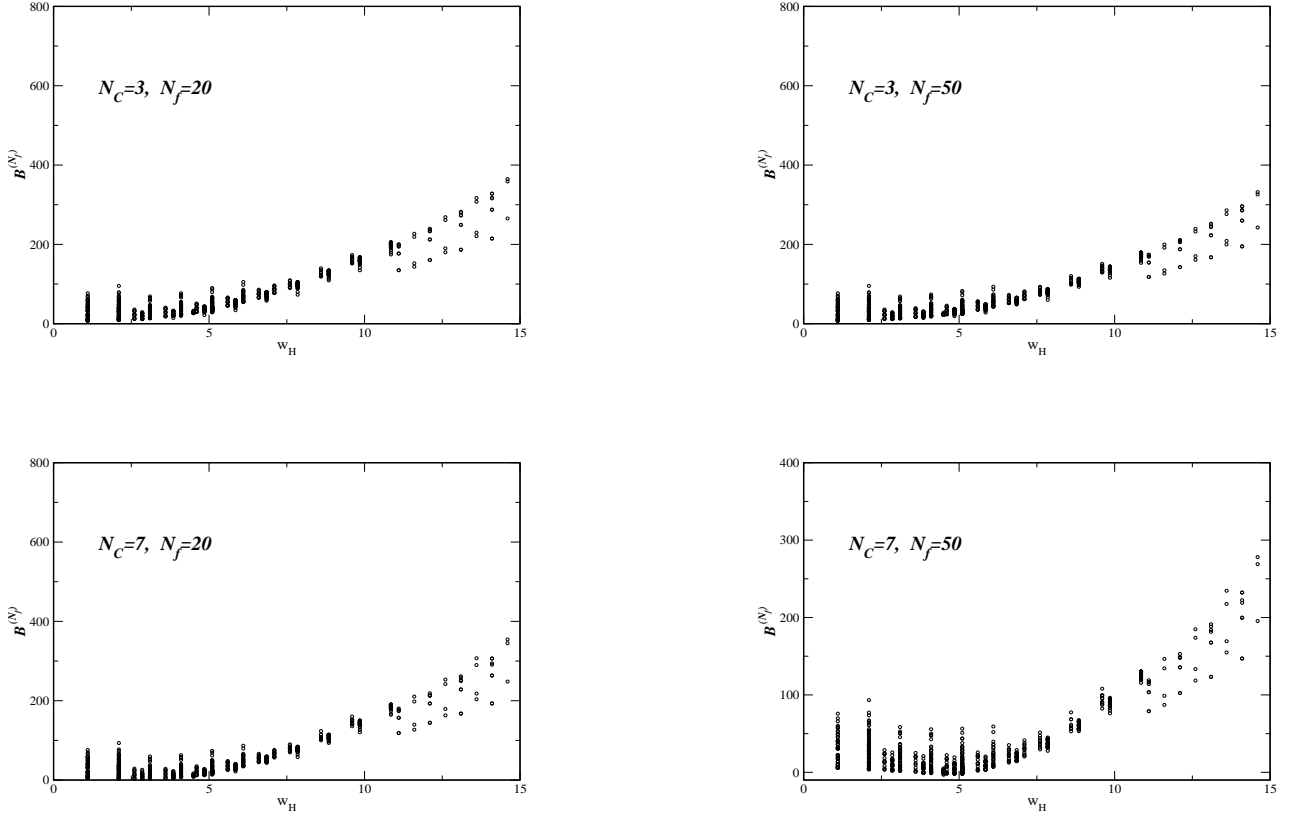


FIG. 6: The binding energy, eq. (4.6) as function of the width parameter w_H for various values of N_C and N_f .

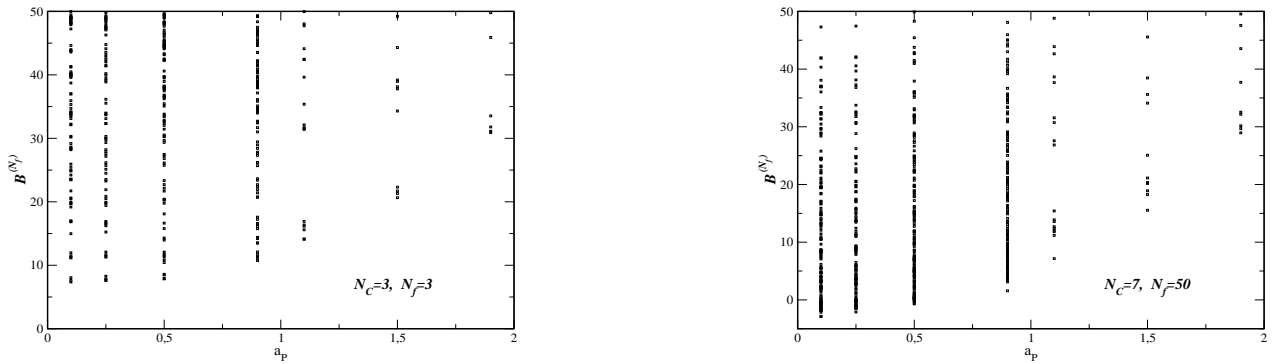


FIG. 7: The binding energy as function of the amplitude of the charged scalar field a_P for two values of the number of populated levels.

the classical energy in comparison to the fermion determinant and bound state contributions. The obvious question is whether there are other regions in the space of model parameters that allow for stable objects. Such a search, of course, cannot be exhaustive and we will therefore just report on a single calculation in that direction. The most obvious change in parameters that enhances the role of the fermion fluctuations is an increase in the Yukawa coupling, f . This change increases the fermion mass and simultaneously decreases the VEV of the Higgs field in $D = 2 + 1$ due to our definition eq. (3.15). Since $v = v_{D=2+1}$ sets the scale of the classical energy, this change represents an additional

enhancement of the fermion vacuum contribution.

In figure 8 we show the resulting binding energy for our choice $m_f = 1.5\text{TeV}$. As expected we do get a bound object for the physical value $N_C = 3$ and a large number of populated fermion levels. It is amusing to see that even a

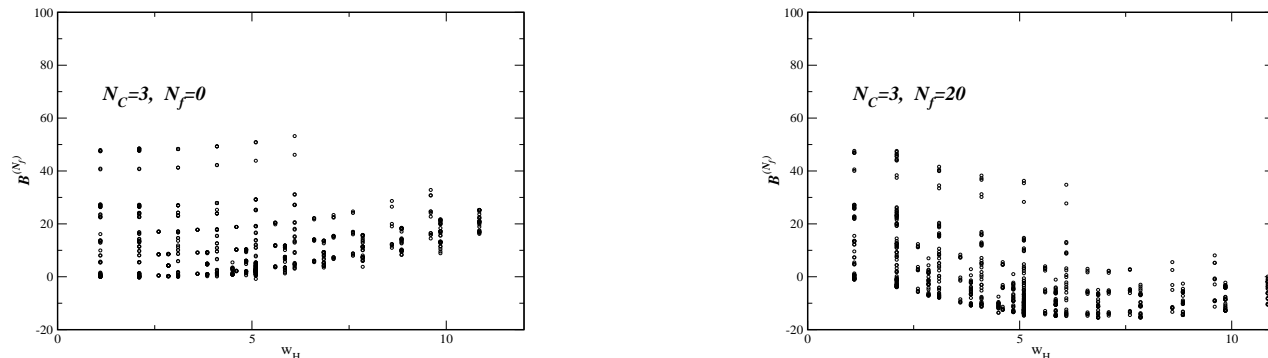


FIG. 8: The binding energy as function of the width of the Higgs field w_H for a large fermion mass, $m_f = 1.5\text{TeV}$ and two values of the number of populated levels.

fermion number zero object ($N_f = 0$) acquires binding. That is, for such large a fermion mass the vacuum becomes unstable already for $N_C = 3$, at least in the one fermion loop approximation. For $m_f = 170\text{GeV}$ we need to tune $N_C \sim 100$ to observe the same effect. Of course, we expect that there exists an intermediate value of the fermion mass between 170GeV and 1.5TeV for the which this vacuum instability sets in for $N_C = 3$.

V. CONCLUSIONS

In this paper we have studied the quantum energies of static and localized W -string configurations in a $D = 2 + 1$ dimensional gauge theory. This is to be understood as a precursor to a full investigation of quantum energies of W/Z -string configurations in the standard model in $D = 3 + 1$. As we know from studies on QED flux tubes, the limitation to $D = 2 + 1$ dimensions is a reliable truncation for string-type configurations when the $D = 3 + 1$ renormalization conditions are imposed and the vacuum expectation value of the Higgs field is suitably scaled.

We have concentrated on the fermion contributions to the vacuum polarization energy as a first calculation that comprehensively compares that energy to the one associated with the the trivial vacuum configuration, where the Higgs field sits at the minimum of its potential and the gauge fields vanish. This approach is motivated by the observation that there exists a fermion zero-mode for field configurations that correspond to the W -string with the charged Higgs field being identically zero. The population of this zero mode could yield a significant energy gain. The incorporation of contributions due to a single fermion mode requires us to also include the full fermion vacuum polarization energy because it is of identical order in both the loop and large N_C expansions, where N_C counts the degeneracy of the fermions, *e.g.* the number of color degrees of freedom. We compute the effective energy as the sum of the classical energy, the bound state contributions and the (renormalized) fermion vacuum polarization energy. In the combined limit, $\hbar \rightarrow 0$ and $N_C \rightarrow \infty$ this approximation becomes exact at next to leading order.

We have employed techniques that use scattering data for the computation of the vacuum polarization energy. These techniques have the important and outstanding feature that standard renormalization conditions, formulated in terms of Green's functions in momentum space, can be straightforwardly imposed. This is essential for a sensible comparison to the energy of the translationally invariant vacuum configuration and to generalize the $D = 2 + 1$ results to $D = 3 + 1$. To make efficient use of this powerful scattering theory approach, however, we have to assume that the fermions in the doublet are degenerate in order to obtain a partial wave expansion. Our numerical results show that this contribution to the total energy is small for configurations of interest, and does not destroy stability of the string.

We have found energetically favored string configurations within an ansatz of variational parameters characterizing the W -string configuration. Although the true minimum likely lies outside our ansatz, its energy can only be less. Though we find that the fermion vacuum polarization energy reduces the effective energy, our numerical results show that the large classical energy carried by the pure W -configuration cannot easily be compensated by fermion quantum contributions with smaller classical energies. Rather, in the search for energetically stable configurations we are led

to Higgs field dominated scenarios. In turn, this result reduces the importance of the zero mode. This is a significant result, one that runs contrary to our expectations and demonstrates that the search for stable configurations requires one to fully account for the fermion spectrum in the string background, rather than merely concentrating on just the zero mode. Furthermore, the change in character of the fields when going from the gauge field dominated to the Higgs field dominated scenarios is quite interesting. In the gauge field dominated case the fields have non-zero winding at infinity and magnetic flux. In the other case we are essentially left with only a shallow ring in coordinate space in which a hole is dug into the Higgs vacuum expectation value.

In the regime of interest, where the extension of the background fields is a few times the Compton wave-length of the fluctuating fermion, the number of bound states essentially grows quadratically with the widths of the background fields. The hole in the Higgs vacuum expectation value causes the corresponding binding. Although these states are generally only weakly bound, they are so numerous that they can cause an object with large fermion number to indeed be bound. Though we did not observe such a configuration for empirically motivated model parameters, we have seen that a doubling of the fermion degeneracy or an increase of the fermion mass provides sufficient emphasis on the fermion contribution to the total energy such that stable objects emerge. Typically these stable objects carry fermion numbers of about one hundred or even more and the configurations are quite wide, a few times the Compton wave-length of the free fermion.

We have not taken the effort to determine a minimal value for the fermion mass for which a stable configuration emerges. However, for the empirical value of the fermion mass the critical value $N_C = 7$ is not too far away from the physical datum. It thus does not seem totally absurd to imagine that in $D = 3 + 1$ a stable object exists when adopting the standard model parameters. This certainly motivates the corresponding extension of the present study, but some technical obstacles must be overcome first. In $D = 2 + 1$ it was sufficient to compute Feynman diagrams (and Born terms) up to second order in the external fields. The expansion with respect to external fields is gauge variant, but only gauge invariant combinations of Higgs and vector fields have well defined Fourier transforms that enter the Feynman diagrams. (The full effective energy is, of course, gauge invariant as the analogous peculiarity is contained in the Born series for the scattering data.) Already in the present case we had to introduce a fake Higgs field to circumvent that problem. Once we go to higher order in the Feynman diagrams, additional manipulations of this kind will be needed. One possibility is to unwind the string configuration at some distant point in space by making the angle ξ_1 in the parameterization, eq. (2.24) space dependent, such that it vanishes at $r \rightarrow \infty$. Unlike in the case of the QED flux tubes the *return flux* associated with 'unwinding' the strings will contribute to the energy even if the distant point is sent to infinity. Though that contribution is easy to estimate (and thus subtract) for the classical energy, it is not so for the vacuum polarization energy, which is a non-local functional of the background fields. We expect, however, that the artificial 'unwinding' part of the effective energy can be quantified by some approximate techniques such as the gradient expansion. Since the present study indicates that $\xi_1 \rightarrow 0$ for the energetically favored configuration, it is also worthwhile to explore pure Higgs background configurations in $D = 3 + 1$. Studies in that direction are in progress.

Acknowledgments

We are very grateful to V. Khemani for helpful cooperation in the early stage of this investigation. O. S. is grateful to the Center of Theoretical Physics at the MIT for hospitality and the Particle Theory Group at the University of Plymouth for a good working atmosphere and interesting discussions.

N. G. was supported by a Cottrell College Science Award from Research Corporation and by National Science Foundation award PHY-0555338. O. S. was supported by the *Deutsche Forschungsgemeinschaft* under grant DFG Schr 749/1-1 and by PPARC.

APPENDIX A: PERTURBATION THEORY

1. Renormalization Conditions

The counterterm Lagrangian for the $SU(2)_L$ model is given by

$$\mathcal{L}_H^{(\text{ct})} = c_1 \text{tr}(W^{\mu\nu} W_{\mu\nu}) + c_2 \left([D^\mu \phi]^\dagger D_\mu \phi \right) + c_3 \left[(\phi^\dagger \phi) - v^2 \right] + c_4 \left[(\phi^\dagger \phi) - v^2 \right]^2. \quad (\text{A1})$$

The counterterm coefficients corresponding to the renormalization conditions outlined in the main text are:

$$c_1 = \frac{g^2}{32\pi m_f} I_1^{(3)}, \quad c_2 = \frac{f^2}{\pi m_f} I_2^{(3)}(\xi_H), \quad c_3 = \frac{1}{\pi} f^2 m_f \quad \text{and} \quad \bar{c}_4 = \frac{2f^2}{\pi} m_f I_4^{(3)}(\xi_H), \quad (\text{A2})$$

with $\bar{c}_4 = 4v^2 c_4 + c_3 + m_H^2 c_2$ and $\xi_H = m_H/m_f$. For all parts of the Feynman diagram calculation we employ dimensional regularization. This is the reason for c_3 being finite, even though it is used to cancel a linear (by power counting) divergence.

The Feynman parameter integrals are given in D=2+1 by:

$$I_1^{(3)}(\xi) = \frac{\xi + (1 - \xi^2/4) \ln \frac{2+\xi}{2-\xi}}{\xi(4 - \xi^2)}, \quad (\text{A3})$$

$$\bar{I}_1^{(3)}(\xi) = 1 + \frac{\xi}{4} \ln \frac{2-\xi}{2+\xi}, \quad (\text{A4})$$

$$I_2^{(3)}(\xi) = \frac{1}{8\xi^3} (4\xi - (4 + \xi^2) \ln \frac{2-\xi}{2+\xi}), \quad (\text{A5})$$

$$I_3^{(3)}(\xi) = \frac{1}{8\xi^2} (4\xi + (4 - \xi^2) \ln \frac{2-\xi}{2+\xi}). \quad (\text{A6})$$

2. The Renormalized Second Order Feynman Diagram

The second order renormalized Feynman diagram involves only the scalar profile functions. It is most easily expressed using the Fourier transforms

$$\tilde{f}_H(k) = \int_0^\infty \rho d\rho J_0(k\rho)(1 - f_H(\rho)) \text{ and } \tilde{f}_P(k) = \int_0^\infty \rho d\rho J_0(k\rho)f_P(\rho). \quad (\text{A7})$$

As discussed at the end of section III E it suffices to consider $\xi_1 = 0$. Then, the contribution to the energy is

$$E^{(2)} = 2m^5 \int_0^\infty \eta d\eta \{ [(\eta^2 + \xi_H^2)I_2(\xi_H) + 2I_4(i\eta) - 2I_4(\xi_H)] \tilde{f}_H^2(m_f\eta) + [\eta^2 I_2(\xi_H) + I_4(i\eta) - 1] \tilde{f}_P^2(m_f\eta) \} \quad (\text{A8})$$

with $\xi_H = m_H/m_f$ and $i\eta$ being a space like momentum fraction.

3. The counterterm contribution to the energy

In this section, we give the contribution of the counterterms to the energy that weren't used in renormalizing the second order Feynman diagram. The energy contribution is

$$E_{c.t.}^{(3,4)} = 2\pi \int \rho d\rho \mathcal{E}_{c.t.} \quad (\text{A9})$$

with

$$\mathcal{E}_{c.t.} = -4c_1 \sin^2(\xi_1^2) \frac{n^2}{g^2} \frac{f_G'^2}{\rho^2} + c_2 v^2 \frac{n^2}{\rho^2} \sin^2 \xi_1 (f_H^2(1 - f_G)^2 + f_P^2 f_G^2) - c_4 v^4 ((1 - f_H^2 - f_P^2)^2 - 4(1 - f_H)^2). \quad (\text{A10})$$

-
- [1] T. Vachaspati, Phys. Rev. Lett. **68**, 1977 (1992).
 - [2] A. Achucarro and T. Vachaspati, Phys. Rept. **327**, 347 (2000), hep-ph/9904229.
 - [3] Y. Nambu, Nucl. Phys. **B130**, 505 (1977).
 - [4] S. G. Naculich, Phys. Rev. Lett. **75**, 998 (1995), hep-ph/9501388.
 - [5] T. W. B. Kibble, J. Phys. A: Math. Gen. **9**, 1387 (1976).
 - [6] M. B. Hindmarsh and T. W. B. Kibble, Rept. Prog. Phys. **58**, 477 (1995), hep-ph/9411342.
 - [7] S. Perlmutter et al. (Supernova Cosmology Project), Astrophys. J. **517**, 565 (1999), astro-ph/9812133.
 - [8] A. G. Riess et al. (Supernova Search Team), Astron. J. **116**, 1009 (1998), astro-ph/9805201.
 - [9] D. Spergel and U.-L. Pen, Astrophys. J. **491**, L67 (1997), astro-ph/9611198.
 - [10] P. McGraw, Phys. Rev. **D57**, 3317 (1998), astro-ph/9706182.
 - [11] M. Bucher and D. N. Spergel, Phys. Rev. **D60**, 043505 (1999), astro-ph/9812022.
 - [12] R. H. Brandenberger and A.-C. Davis, Phys. Lett. **B308**, 79 (1993), astro-ph/9206001.

- [13] F. R. Klinkhamer and C. Rupp, J. Math. Phys. **44**, 3619 (2003), hep-th/0304167.
- [14] E. D'Hoker and E. Farhi, Nucl. Phys. **B248**, 59 (1984).
- [15] E. D'Hoker and E. Farhi, Nucl. Phys. **B248**, 77 (1984).
- [16] M. Groves and W. B. Perkins, Nucl. Phys. **B573**, 449 (2000), hep-ph/9908416.
- [17] N. Graham, R. L. Jaffe, and H. Weigel, Int. J. Mod. Phys. **A17**, 846 (2002), hep-th/0201148.
- [18] N. Graham, V. Khemani, M. Quandt, O. Schroeder, and H. Weigel, Nucl. Phys. **B707**, 233 (2005), hep-th/0410171.
- [19] N. Graham, R. L. Jaffe, M. Quandt, and H. Weigel, Phys. Rev. Lett. **87**, 131601 (2001), hep-th/0103010.
- [20] O. Schroeder, J. Phys. **A39**, 6733 (2006), hep-th/0601196.
- [21] H. B. Nielsen and P. Olesen, Nucl. Phys. **B61**, 45 (1973).
- [22] H. Reinhardt, Nucl. Phys. **B503**, 505 (1997).
- [23] M. Quandt, H. Reinhardt, and A. Schaefer, Phys. Lett. **B446**, 290 (1999).
- [24] F. R. Klinkhamer and P. Olesen, Nucl. Phys. **B422**, 227 (1994), hep-ph/9402207.
- [25] V. Khemani (2004), hep-th/0404234.
- [26] H. Weigel, B. Schwesinger, and G. Holzwarth, Phys. Lett. **B168**, 321 (1986).
- [27] E. Farhi, N. Graham, R. L. Jaffe, V. Khemani, and H. Weigel, Nucl. Phys. **B665**, 623 (2003), hep-th/0303159.
- [28] E. Farhi, N. Graham, P. Haagsen, and R. L. Jaffe, Phys. Lett. **B427**, 334 (1998), hep-th/9802015.
- [29] N. Graham and R. L. Jaffe, Nucl. Phys. **B549**, 516 (1999), hep-th/9901023.
- [30] J. Schwinger, Phys. Rev. **94**, 1362 (1954).
- [31] N. Graham et al., Nucl. Phys. **B645**, 49 (2002), hep-th/0207120.
- [32] I. J. R. Aitchison and C. M. Fraser, Phys. Lett. **B146**, 63 (1984).
- [33] I. J. R. Aitchison and C. M. Fraser, Phys. Rev. **D31**, 2605 (1985).